DESIGN AND FABRICATION OF A STRESSED-MANAGED Nb_3Sn WIND AND REACT DIPOLE

A Thesis

by

PATRICK DANIEL NOYES

Submitted to the Office of Graduate Studies of
Texas A&M University
in partial fulfillment of the requirements for the degree of

MASTER OF SCIENCE

May 2007

Major Subject: Physics

DESIGN AND FABRICATION OF A STRESSED-MANAGED Nb_3Sn WIND AND REACT DIPOLE

A Thesis

by

PATRICK DANIEL NOYES

Submitted to the Office of Graduate Studies of
Texas A&M University
in partial fulfillment of the requirements for the degree of

MASTER OF SCIENCE

Approved by:

Chair of Committee,	Peter McIntyre
Committee Members,	Robert Kenefick
	Mehrdad Ehsani
Head of Department,	Edward Fry

May 2007

Major Subject: Physics

ABSTRACT

Design and Fabrication of a Stressed-Managed Nb_3Sn Wind and React Dipole.

(May 2007)

Patrick Daniel Noyes, B.S., Texas A&M University

Chair of Advisory Committee: Dr. Peter McIntyre

A new approach to high-field dipole design is being developed at Texas A&M University. The goal of the development is to facilitate the use of high-field conductors (Nb3 and Bi-2212) and to manage Lorentz stress and magnetization so that field strength can be extended to 25 Tesla. The new design incorporates several innovations, including stress management, flux plate suppression of multipoles, and bladder preload. A series of model dipoles is being built and tested to validate and optimize each of these innovations. The second such model dipole, TAMU2, has been completed and was recently tested at Lawrence Berkeley National Laboritory. It achieved 93% of cable short sample limit on the first quench and every subsequent quench and did not suffer from any detectable training. This level of performance corrisponds to currents over 8800 A and a measureable field strength of 4.6 T. Ramp rate studies indicate robust behavior under fast ramping; we interpret this to be a beneficial result of the block coil geometry and the chrome-plated conductor.

TABLE OF CONTENTS

Page

1. INTRODUCTION 1

1.1. High Field Dipoles 2
1.2. Rapid Ramping Dipoles 3

2. DESIGN REQUIREMENTS 5

2.1. Field Strength 5
2.2. Coil Geometry: Block Coil, Cosine-Theta Coil, Common Coil 8
2.3. Aperture 12
2.4. Field Quality 12
2.5. Ramp Rate and AC Losses 17

3. TAMU SERIES DIPOLE DESIGN 19

3.1. Stress Management 19
3.1.1. Piers and Beams 20
3.1.2. Springs 21
3.1.3. Coil Loading 22
3.1.4. Bladder Preload 23
3.1.5. Friction-locked Ends 24
3.1.6. Conductor Grading 24
3.2. Gapping Element 25
3.3. Flux Plate 25

4. TAMU2 MAGNET FABRICATION 27

4.1. ITER 622 Conductor 27
4.2. Cable Wash 28
4.3. Ten Stack Test 30
4.4. Coil Winding 31
4.5. Reaction Bake 34
4.6. Splicing 40
4.7. Ground Plane Installation 42
4.8. Epoxy Impregnation 44
4.9. Final Loading 45
4.10. Instrumentation 51
4.11. Setup for testing at Lawrence Berkeley National Lab 53

5. TESTS AND RESULTS 56

5.1. Training Curve 56
5.2. Quench Location 58
5.3. Field Strength 59
5.4. Ramp Rate Study 60
5.5. Splices 60
5.6. Coil End Loads 61
5.7. Lorentz Side Loads 62

Page

5.8. TAMU2 Cross-Section Study 62
5.9. Transducer Tests 63

6. LESSONS 64

6.1. Fabrication Lessons 64
6.1.1. Omega Temperature Controller 64
6.1.2. Gasket Seals 65
6.1.3. Coiled Copper Inflation Lines 65
6.2. Changes to be Applied to TAMU3 66
6.2.1. Oven Related Pier Damage 66
6.2.2. Coil Position within the Flux Return Laminations 66
6.2.3. Potential Conductor Strain due to RTV in Mandrel Gap 66
6.2.4. Transducer Calibration Issues 67

7. CONCLUSION 68

REFERENCES 69

VITA 71

LIST OF TABLES

TABLE Page

1.1 Basic Parameters of the Tevatron and LHC..... 2

4.1 Measurement of material removed from coil during reaction bake……..... 38

5.1 Calculated possible stress levels and measured value for the ends of the magnet.……..……..…… 61

LIST OF FIGURES

FIGURE		Page
2.1	Jc measurements of various conductors…….…….	5
2.2	Recent Nb3Sn model dipole records……	6
2.3	Comparison of the strain sensitivity of Nb3Sn to that of NbTi……	7
2.4	Visual comparison of filament sizes…….……	8
2.5	Cross-section of the first block dipole…….…….	9
2.6	Field calculation of a block dipole at 14 T…..……..……	10
2.7	Diagram of the Cosine Theta magnet MSUT……..…….	11
2.8	Low field calculation of a block dipole at 0.5 T with the iron unsaturated……..……..……	13
2.9	High field calculation of block dipole at 14 T…….....……	14
2.10	Flux return assembly diagram……..……....……	14
2.11	Diagram of current types…….…...…….….	15
2.12	LHC snap back measurements…...…….…...……..……	16
2.13	Dependence of the critical field on the ramp rate for the magnet MSUT……...……	17
3.1	Diagram of TAMU4 with stress management components labeled…...…	20
3.2	Calculation of the mechanical stresses in TAMU4……..……	21
3.3	Fixtures for fabricating springs as well as two straight springs.……..…	22
3.4	Laminated titanium mandrel……	23
3.5	Vertical preload…….……..……	24
3.6	Three dimensional asymmetric calculation of TAMU2…..…….....…….	25
3.7	Flux plate effects…….....…….....…….	26
4.1	ITER conductor samples……..…….……..….	27
4.2	Cross section of ITER622 conductor…….....…….……..	28
4.3	S-glass preparation…….…….……	29
4.4	Palmitic acid application……..…….……..……	30
4.5	Spring preload……..……..……..……	31

FIGURE Page

4.6 Location of the voltage taps in TAMU2…….. 32
4.7 Leaf shims and their locations…….. 32
4.8 Torch cutting mica…….. 33
4.9 Mica plane installed on top of the outer coil on the left…….. 33
4.10 Titanium mandrel just before winding…….. 34
4.11 Furnace base with the coffin set on top…….. 35
4.12 Oven assembled with the jar suspended from the crane…….. 35
4.13 Coffin extraction from the fur…….. 36
4.14 Graph of the total reaction bake cycle…….. 39
4.15 Pier damage just after reaction bake…….. 39
4.16 RTV jammed in the gap of the mandrel…….. 40
4.17 Splicing steps…….. 42
4.18 Installation of the protection heaters and voltage tap traces……..... 43
4.19 Capacitive pressure transducer…….. 43
4.20 Vacuum impregnation…….. 45
4.21 Bladder preload……..... 46
4.22 Steel lamination assembly…….. 47
4.23 Flux return halves are installed in a vertical position into the cylinder…….. 48
4.24 Pressurization of the bladders with the coil and magnetic mirror installed…….49
4.25 Large grains are formed when the Woods metal is cooled too quickly…… 50
4.26 Hot water manifold…….. 50
4.27 Bolt strain gauges on the ends of the magnet…… 51
4.28 Electrical problems with the coil at 300 K…….. 53
5.1 Graph of time (ms) versus the rate of change of the voltage during quench test four..... 57
5.2 TAMU2 quench history……... 58

FIGURE Page

5.3 Location where the spontaneous quench began during the standard quench tests……..…….…….. 59
5.4 Load line graph for TAMU2……...……. 59
5.5 Power supply fluctuations…… 60

1. INTRODUCTION

In the past few decades there have been many important discoveries in particle physics. These discoveries were heavily dependent on the accelerator technologies that allowed for pushing the performance envelope of the machines reference. Many of the parameters of these accelerators that achieve higher energies than a simple electrostatic accelerator rely directly on the capabilities of the magnets used in the design. Magnets are used in charged particle beam optics much like lenses and prisms are used to control beams of photons. As more powerful fields and gradients were required to achieve higher beam energies and luminosities, the move to replace resistive magnets with superconducting magnets became the obvious logical choice reference. This is predominantly due to the enormous electrical budget that would be required for a high energy resistive accelerator over the lifetime of the machine. Building much more expensive, but dramatically lower operating cost, superconducting magnets is an easy economic choice.

To build the next high energy hadron collider there are two approaches that may be taken to increase the beam energy beyond that which is currently available. A larger diameter machine would produce higher energies using the same magnet technology although the cost would roughly scale with the beam energy. The second approach would be to increase the magnetic field strength inside the dipoles which bend the beam on a circular trajectory. In reality these two approaches are both optimized for the targeted energy which the accelerator is to achieve. The energy of a synchrotron is given roughly by the equation:

$$p = .3BR. \tag{1.1}$$

This thesis follows the style of *IEEE Transactions on Applied Superconductivity.*

B is the field strength in Tesla, R is the radius of the machine in meters, and p is the momentum of the particles in GeV/c. The LHC, which is due to come online in 2007, takes advantage of both these approaches when compared to the Tevatron. Various parameters are given in table 1.1.

Table 1.1

Basic parameters of the Tevatron and LHC.

	Tevatron	LHC	
Radius	1000	2800	m
Dipole field strength	4.2	8.33	T
Beam energy	.98	7	TeV

In the quest to understand on a more fundamental level the world in which we live, higher energy accelerators are required. There are currently a number of questions that could be answered at higher energy accelerators than are available today. Some of the questions are:

- Do supersymmetric particles exist?
- What is dark matter?
- Why is there more matter than antimatter?

1.1. High Field Dipoles

A major technical challenge for higher energy machines is to build higher field dipole magnets. This development path has led from resistive magnets used in the Bevatron [1], CERN PS, and Fermilab Main Ring to the current-generation superconducting magnets in the Tevatron and LHC [2]. Those superconducting magnets use cables of NbTi conductor. When a coil of NbTi cable with ~5 cm^2 cross-section is cooled to the temperature of liquid helium (4.2 K) it can carry the ~million ampere turns

needed to make a magnetic field up to ~8 Tesla without any electrical resistance. If the cables are arranged in a cosine-theta geometry around a circular beam tube, a uniform dipole field is produced in its interior.

As the magnetic field in a superconductor increases, the fraction of electrons that form Cooper pairs decreases and reaches zero at the upper critical field H_{c2}. The upper critical field of NbTi is ~10 T, and so the maximum field that can be produced using coils is ~8 T (the field of the LHC dipoles). Developments in field strength over the past fifteen years have pushed the performance required of the conductor well past what NbTi is capable of. The conductor Nb_3Sn has an upper critical field ~26 T, and has been used in most development of high-field dipoles during the past decade. As discussed below, the cosine-theta geometry has been replaced in most recent work by a geometries that better accommodate immense Lorentz stresses within the coil; both common coil[3] [4] and block coil [5] [6]designs have been developed. In the future, conductors with even higher H_{c2} such as MgB_2, or Bi-2212 may be employed to push dipole field beyond 20 Tesla.

An important property of all such high-field superconductors is that they are brittle. A 16 Tesla dipole produces Lorentz stress of at least 150 MPa inside the windings, so great care must be taken to control the Lorentz forces that are present. To use Nb_3Sn in high-field dipoles, the Lorentz forces must be carefully controlled within the allowable limits of the material. The model block-coil dipole HD1 [7], built by LBL, currently holds the world record for dipole field strength at just over 16 T.

1.2. Rapid Ramping Dipoles

An equally challenging frontier that is currently being developed in the superconducting magnet field, is the rapid ramping dipole. There is a need for rapid ramping dipoles that are capable of achieving up to 4 T/s ramp rates [8]. The field is not as high as the high field dipoles and so are not placed under the same immense loads, but they do cycle much more often and therefore must deal with other mechanical difficulties.

Mechanical difficulties arise from material fatigue. Rapid cycle dipoles could see well in excess of a million cycles per year. These magnets will still be exposed to relatively high forces and therefore crack propagation becomes a very important issue to solve.

The large number of cycles in a fairly short time also equates to tremendous changes in flux inside the magnet. This change in flux causes large eddy currents to form due to Lenz's law, which are problematic in two ways. These currents flow through resistive regions in the coil and are most intense at the peak field regions in the magnet. This is where the superconductor is running closest to its margin and the additional heat can easily initiate a quench. A large amount of heat will also be dispersed throughout the magnet and may cause serious refrigeration issues. The eddy currents will also counteract the magnetic field itself which will alter the quality of the field.

Rapid ramping dipoles would be used for the investigation of phenomena pertaining to heavy ion experiments. These range from:

- Nuclear structure experiments performed with cooled beams of short lived nuclei,
- Atomic physics experiments with high-Z ions in a wide range of energies,
- Investigation of the properties and evolution of hot dense plasmas.

2. DESIGN REQUIREMENTS

2.1. Field Strength

The most important parameter to increase in the development of future hadron colliding synchrotrons is the dipole field strength. An increase in field strength leads directly to higher energy machines which are critical for future experiments.

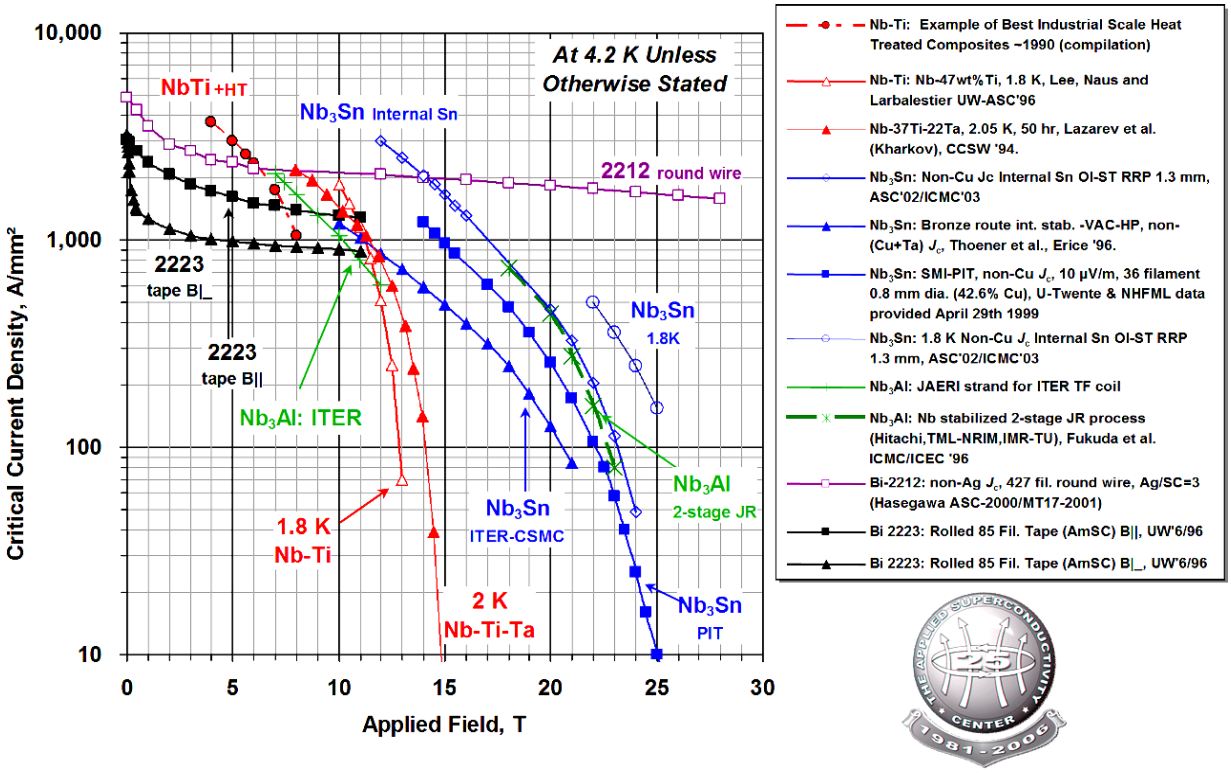

Fig. 2.1. J_c measurements of various conductors. Graph of the field strength at which given return to a resistive state at given current density. Image courtesy of Peter J. Lee of the Applied Superconductivity Center, copyright retained.

The conductor of choice for every superconducting high energy machine since the Tevatron has been NbTi. This conductor is very mechanically robust and has offered excellent performance in current machines. Despite this, the LHC should be the last high energy machine to primarily use NbTi in its high field dipoles due to the amount of

current that it is capable of carrying at higher fields as shown in figure 2.1. In order to reach the field of 8.33T reliably, the operating temperature must be reduced to 1.9K [2].

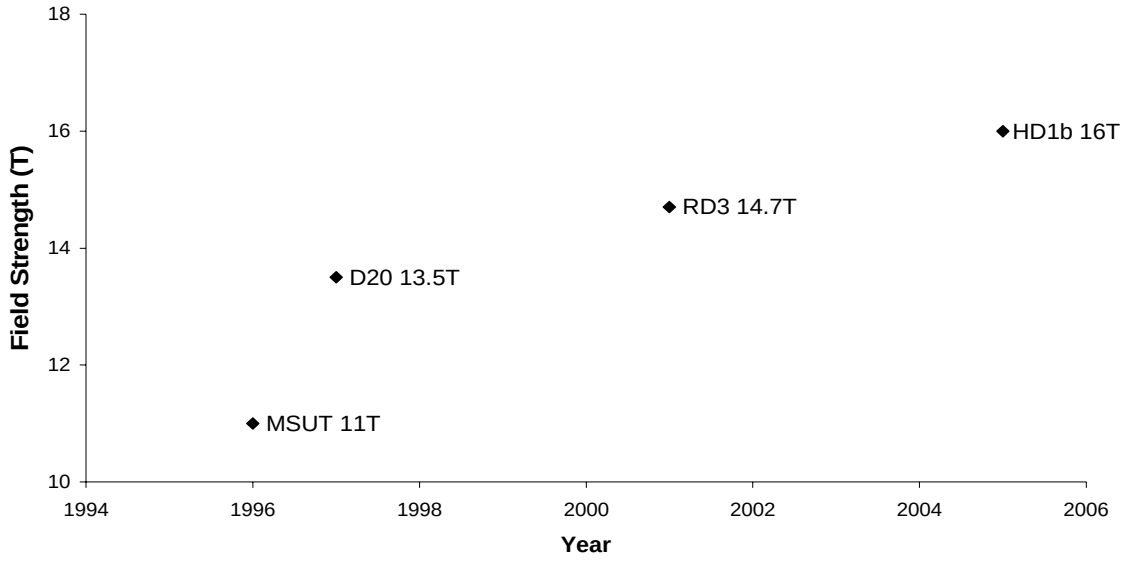

Fig. 2.2. Recent Nb_3Sn model dipole records.

The move to higher field strengths requires a conductor with superior electrical properties. Currently, high field dipole research programs utilize Nb_3Sn in the high field regions of the magnets. The move to Nb_3Sn has been due to its electrical performance which is far superior to that of NbTi and as a direct result, every record breaking dipole has used Nb_3Sn for the past ten years as shown in figure 2.2. Recent advances in manufacturing have made Nb_3Sn an even more attractive choice. Dipoles, such as LBL's D20, used a conductor that measured 900 A/mm^2 at 4.4 K and a 12 T background field. The current state of the art is 3000 A/mm^2 and it is projected that current densities of 4000 A/mm^2 should be attainable [9]. Not only is Nb_3Sn superior to NbTi in the presence of a background field, but its critical temperature is considerably higher at 18 K. This makes it an excellent candidate for rapid ramping dipoles as well.

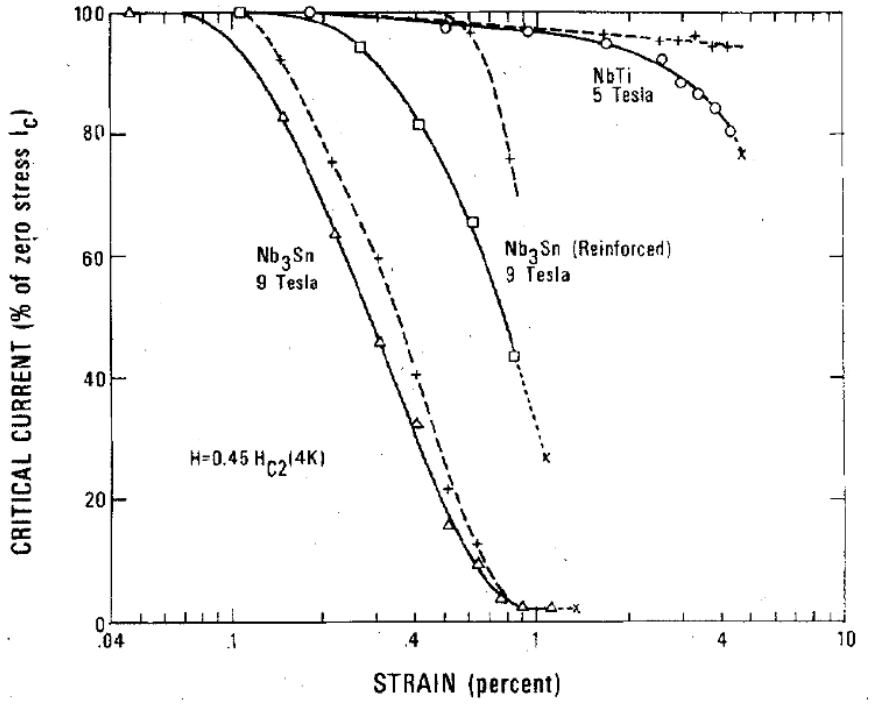

Fig. 2.3. Comparison of the strain sensitivity of Nb_3Sn to that of NbTi.*

Despite its enormous advantages, the move to Nb_3Sn has been hampered by its mechanical properties. The conductor has an A15 structure which is very sensitive to strain degradation shown in figure 2.3. This is further aggravated by the fact that the support for the superconducting filaments is annealed copper. A typical Rutherford cable can withstand 150 MPa of compression before the filaments are irreversibly damaged [10]. As the field strengths increase in the dipoles, this degradation becomes more of a challenge. Fabrication techniques must be adjusted to accommodate its brittle nature. Any design with a small bending radius must use a wind and react approach which means that all magnet components must be able to withstand the 650 °C temperature at which Nb_3Sn is formed. Cable key-stoning must be greatly reduced, if not eliminated completely from the designs as well. Perhaps the most critical locations

* Fig. 2.3 reprinted with permission from "Mechanisms for Critical-Current in NbTi and Nb_3Sn Multifilamentary Wires" by J. W. Ekin, 1977. *IEEE Transactions on Magnetic,* Vol MAG-13, 127-130. 1977 by IEEE.

of a Nb_3Sn dipole are the magnet leads. They must be carefully protected at all times after the conductor has been heat treated to form the Nb_3Sn phase.

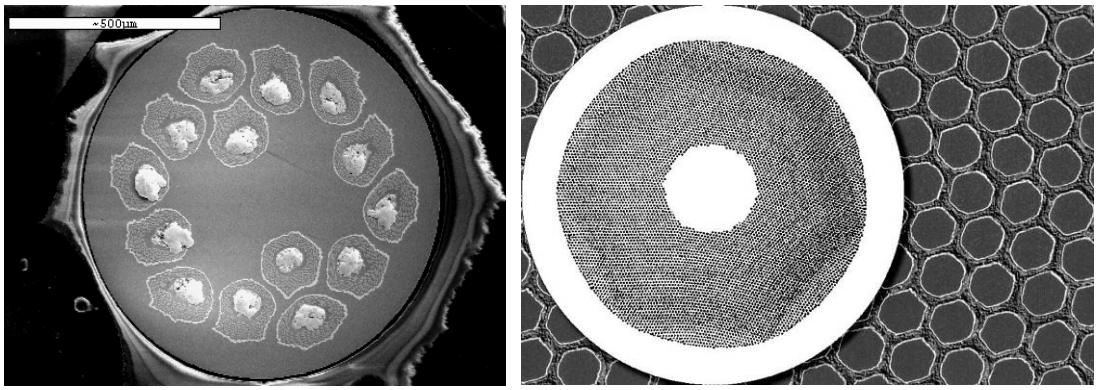

Fig. 2.4. Visual comparison of filament sizes. Left: Iter622 Nb_3Sn conductor with large effective filament size and voids from the bronzing process. Right: NbTi made for the SSC with much finer filaments. SSC conductor image courtesy of Peter J. Lee of the Applied Superconductivity Center, copyright retained.

A second drawback of Nb_3Sn is its filament size. NbTi can be drawn down in the fabrication process to very small sizes. Filaments that are as small as 10µm are common and an effort is underway to reach a filament size of 3.5 µm [11]. Nb_3Sn, however, has a much larger filament size which can range from 100-150µm. As seen in figure 2.4, this large filament size has a degrading effect on the field quality of a magnet. The larger filament supports much larger persistent current multipole strengths which scale proportionally with size.

2.2. Coil Geometry: Block Coil, Cosine-Theta Coil, Common Coil

The TAMU series of dipoles has opted for different geometry than what is currently used in today's particle accelerators. This geometry is known as a block dipole. It was first proposed Dr. W. Sampson in 1977; figure 2.5 shows a cross-section of a block-coil dipole built at BNL at that time.

Fig. 2.5. Cross-section of the first block dipole.

Many of the block dipole advantages stem from the orientation of the conductor. The most important of these advantages is how the conductor intercepts the Lorentz loads. This is done in the most mechanically stable direction possible which is on the wide face of the conductor, thus allowing the internal support come directly from compressing the copper. Taking the loads on the narrow edge, as is done in cosine-theta and common coil dipoles, forces the conductor to bow out in the middle regions and de-cable, since the internal support comes from narrow unstable annealed copper columns.

The difference in internal support within the conductor allows for a completely different strategy when preloading a magnet. Magnets have typically required tremendous amounts of preload which is applied directly onto the windings [12]. The preload is set to slightly greater than the highest Lorentz load that the magnet will see. This places an upper limit on the amount of preload possible to slightly lower than the pressure required to extrude annealed copper, which in turn limits the field possible.

Another major advantage stemming from the conductor orientation is the reduction of AC losses, which has made rapid cycling dipoles a very challenging problem. In the high field regions, where the conductor is running closest to its margin, the conductor presents a minimal profile to the field lines. This minimized profile greatly reduces the amount of flux passing through a single winding. The reduction of flux prevents a

significant a heat build up as the magnet ramps. This is a result of the change in flux that directly heats the cable is directly proportional to the area times the change in field density per unit time. Figure 2.6 shows the minimized area exposed in the high field regions.

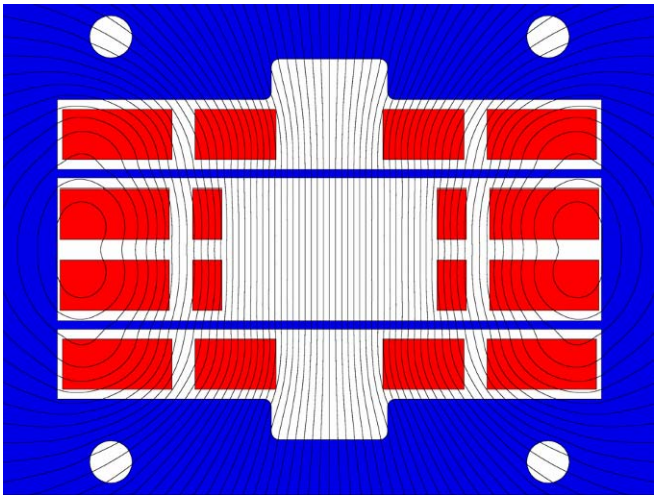

Fig. 2.6. Field calculation of a block dipole at 14 T. The conductor is oriented in the vertical direction in this design.

The block dipole has noticeable fabrication advantages over a cosine-theta magnet as well. The block dipole is a very modular design. This allows for multiple windings to be fabricated in parallel as the windings are not assembled into a magnet until the final step. This feature also allows for individual defective windings to be removed and replaced from a magnet with minimal effort.

Cos θ magnets require special wedge shaped shims and key-stoning of the conductor in order to approximate mathematical ideals. These must be implemented more aggressively as the field strength increases and the aperture sizes are reduced. The wedge shims take valuable space near the aperture which becomes more of a problem with smaller apertures. Key-stoning the conductor also becomes much more of a

problem with Nb_3Sn as the internals can easily be damaged, even with unreacted conductor.

The University of Twente in the Netherlands and LBL have both constructed high field Nb_3Sn cosine-theta dipoles. D20 [13] from LBL is the current world record holder for a cosine-theta dipole but is fairly complex. Four shells of conductor compromise D20, which makes mass production difficult. Twente's dipole MSUT [14] reached 11.5 T, which is not as high as D20, with two shells of conductor shown in figure 2.7. This is a much more practical magnet, but it is unlikely that cosine-theta style dipoles will progress much beyond these two model dipoles in terms of field strength.

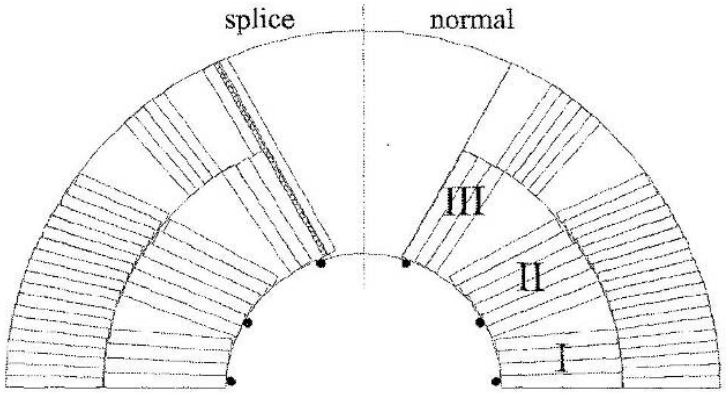

Fig. 2.7. Diagram of the Cosine Theta magnet MSUT.*

The primary advantage that the cosine-theta geometry has held in the past is that of conductor efficiency. With the dipole cost forming a sizable fraction of the overall cost of a new machine, the amount of conductor used in the dipoles is of great importance in minimizing cost. The cosine-theta looses its advantage over the block dipole with smaller apertures.

* Fig. 2.7 Reprinted with permission from "Application of Nb3Sn Superconductors in High-Field Accelerator Magnets" by Andries den Ouden, et al., 1997. *IEEE Transactions on Applied Superconductivity*, Vol 7, 733-738. 1997 by IEEE.

The block dipole geometry is critical to the innovations that are currently under development for the TAMU series of dipole magnets. The block dipole provides a plane above and below the aperture for the flux plate. The geometry is also required for the stress management strategies described in Section 3.

2.3. Aperture

The dynamic aperture of a magnet, which is typically smaller than the physical aperture, is the cross-section of the magnet in which the particle bunches may travel without being destabilized. It is important to increase the dynamic aperture radius as close to the physical aperture radius as possible to minimize the unusable high field region. This minimization reduces the stored energy in the magnet itself and allows for the conductor to physically be positioned closer to the usable field region. A closer physical proximity allows for the magnet field strength to be a higher fraction of the high field point of the magnet.

The aperture is the physical diameter of the bore which contains the beam pipe. This size determines many of the parameters of the magnet [15]. These parameters include conductor cross section, stored energy, and inductance. Reducing the physical aperture is important to bring both fabrication and operating costs down. The Tevatron, for example, has a physical aperture of 76.2 mm but only a dynamic aperture of 50 mm [16].

2.4. Field Quality

Without a high quality magnetic field in the arc dipoles, the strength of that field is of no use for a particle accelerator. A current distribution that is mathematically perfect is unattainable in the real world as we know it and as a result a series of multipoles will arise in the field. This expansion begins with the dipole term and continues through quadrapole and sextapoles terms and beyond [17].

$$B_r + iB_\varphi = B_0 \sum_{n=1}^{\infty} b_n \left(\frac{r}{r_0} \right)^n e^{in\varphi} \qquad (2.2)$$

For the magnetic field to be considered accelerator quality, the coefficients b_n of all multipoles n>1 must be $<10^{-4}$ for a normalization radius r_0 = 1 cm [17]. Even multipoles are suppressed due to the left-right symmetry of the coil and steel.

Odd-order multipoles can arise from a number of sources: placement of cable elements in the winding (structure multipoles), saturation of the steel flux return (saturation multipoles), and magnetization currents induced in the superconductor cables as the magnet is cycled from low to high field to accelerate the beam (persistent multipoles and AC transients).

In designing a dipole to meet the field quality requirement for a collider, design progresses by iterating three steps. Figure 2.8 shows the field during injection. The field lines are dominated by the structural steel pieces used in coil construction as the iron is unsaturated. The multipoles in this region are adjusted by proper placement and dimensioning of the steel.

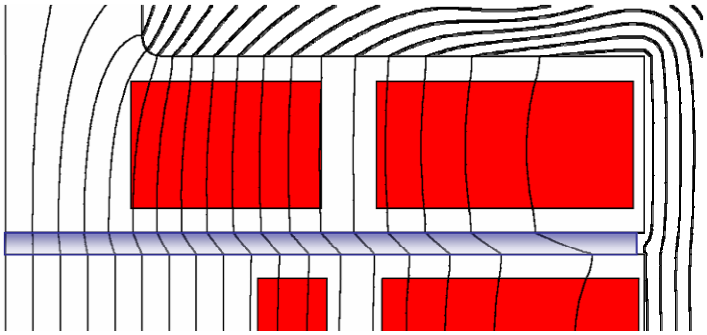

Fig. 2.8. Low field calculation of a block dipole at 0.5 T with the iron unsaturated. This design of block dipole has a steel flux plate, blue, which enforces a dipole boundary condition on the field in the aperature.

At high fields, shown in figure 2.9, the regions of steel nearest the beam tube are saturated (permeability of steel is ~7000 at low field, 100 at 1.3 T, 3 at 2 Tesla), so that the arrangement of cable elements nearest the beam tube largely determines dominates the field distribution. The tolerances on conductor placement determine the multipole field errors.

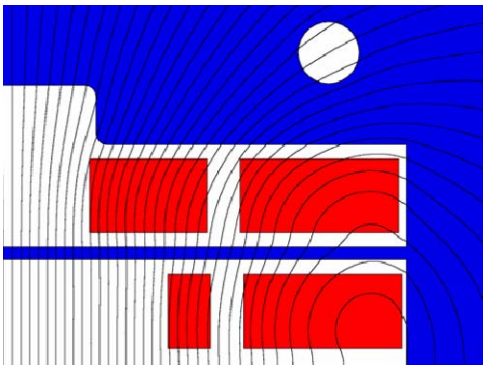

Fig. 2.9. High field calculation of block dipole at 14 T.

As the magnet is energized it passes through a middle region between high and low field strengths, for which the steel nearest the aperture is saturated while most of the steel flux return is not. As field is increased the saturation front moves outward. In this middle region the multipoles are commonly adjusted by the addition of holes in the flux return, which have no effect at low field but control the redistribution of flux as the saturation front passes the location of each hole. Figure 2.10 shows these holes in red.

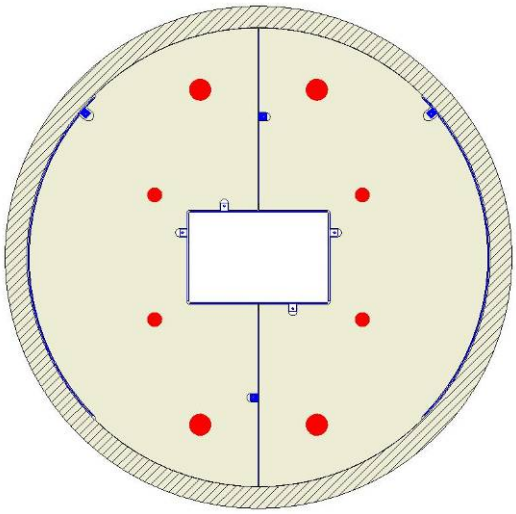

Fig. 2.10. Flux return assembly diagram. The holes, in red, in the flux return assembly are for magnetic design.

Within the conductor itself, errors in the field can arise. These distortions in field distribution can have exceedingly long life times as they are within a superconducting filament, low resistance copper, or both. All of these errors arise on different scales and have different strengths but they are all driven a flux change and are described by Lenz's law. The filaments themselves exhibit a diamagnetic behavior [18]. This is caused by small current loops within the filament. On a slightly larger scale, the strands can exhibit a diamagnetic behavior as well. The current loops are carried across the filaments within the strand. The dominating error arises from the coupling currents between the strands in the conductor. These boundary-induced coupling currents (BICCs) have a greater effect on the quality due to the relatively large area they encompass. The current in a BICC is carried through the superconducting filament almost entirely. This can give them a long lifetime which can reach times on the order of 10^5 s. The only region where the current of the BICC passes through a resistive material is where two strands cross. A BICC is localized one area by the fact that the adjacent BICCs are of opposite sign. A hypothetical two strand conductor is illustrated below in figure 2.11.

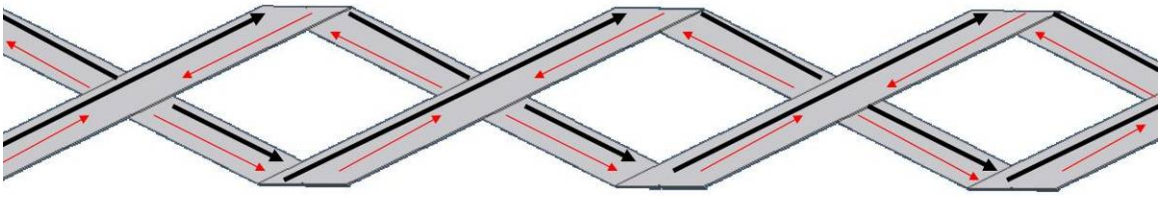

Fig. 2.11. Diagram of current types. Transport current, in black, travels down the length of the cable, while coupling currents, in red, generate current loops in the cable causing magnetization effects.

A major problem which did not arise until superconductors were used in magnets is now known as snapback [19, 20]. This phenomenon was discovered in the Tevatron and can not be corrected with additional corrective magnets. Snapback must be minimized in the design stage of the magnet and is a result of the history of the magnet due to

shielded currents. On the second and subsequent cycles, the magnet is held at a relatively low field for beam injection. During this phase of constant field the magnetization effects of the conductor slowly decay. The decay of the magnetization occurs at a rate defined by the lifetimes of the effects. Once the magnet resumes its ramp to high field the magnetization immediately moves back to the previous curve due to the resuming of the constant flux change. This sudden shift in the sextapole strength, shown in figure 2.12, is caused by suddenly driving the BICCs back to full strength. Due to their domination of the magnetization the previous curve is almost completely recovered. This sudden shift of field can easily destabilize the beam making an abort necessary.

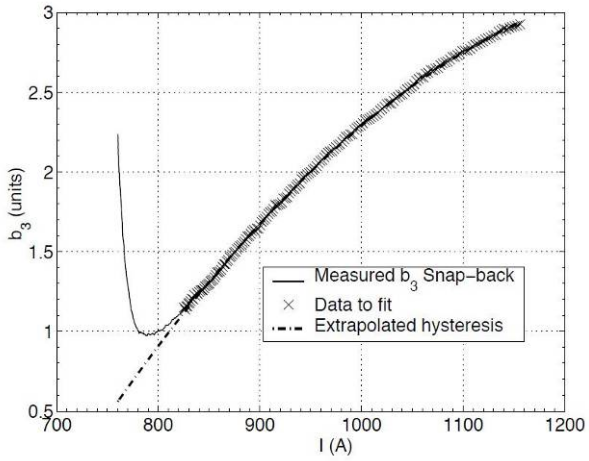

Fig. 2.12. LHC dipole snap-back measurements. Measure of the sextapole moment of the field as the magnet resumes ramping after holding at 750 A.*

* Reprinted with permission from "A Scaling Law for Predicting Snap-Back in Superconducting Accelerator Magnets" by L. Bottura, et al., 2004. *Proceedings of EPAC 2004*, 1609-1611. 2004 by IEEE.

2.5. Ramp Rate and AC Losses

An area of dipole development that has posed considerable challenges is high ramp rates. The higher the ramp rate, the less time that is allowed for cooling of the conductor. Heat is generated both in the conductor and throughout the magnet which can push the conductor past its performance envelope, causing a quench, shown in figure 2.13, and placing an additional load on the refrigeration systems. These heat loads are known as AC losses and arise in three areas throughout the magnet.

The easiest of the AC losses to understand occurs as simple current loops inside the conductor. These loops are essentially the coupling currents previously discussed. Of concern are the BICCs which have relatively short lifetimes and will impart a ΔQ on the conductor. If the heat can not be removed quickly enough, the magnet will quench well below its maximum I_Q. This effect can be reduced, which is discussed later.

The other heat load on the conductor due to AC losses comes from the nature of the superconductor. Inside each filament there are shielded currents from the magnet's history which are not observable. At low transport current levels, the current is carried on the outside surface of the conductor and does not affect the shielded currents inside. As the transport current increases, when the magnet is ramped, the current begins to permeate the filament. When the transport current and shielded current together are beyond what the conductor can handle, a micro quench occurs that eliminates the shielded current. The removal of the shielded currents in this fashion places an additional heat load on the conductor.

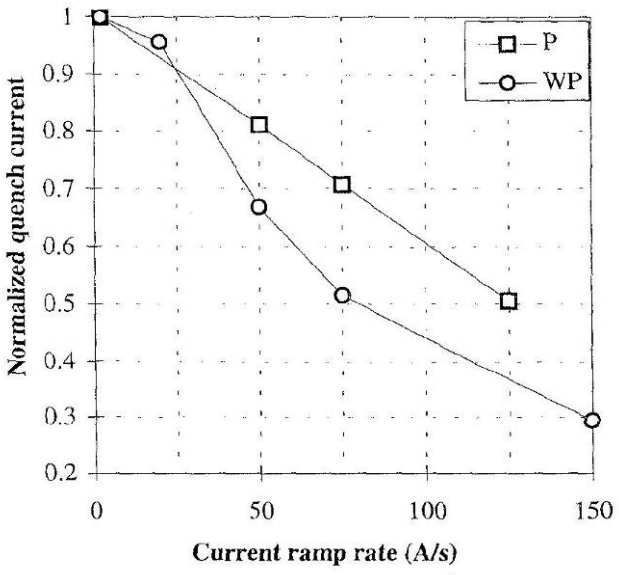

Fig. 2.13. Dependence of the critical field on the ramp rate for the magnet MSUT.*

The final area of AC losses does not directly affect the quench current but does determine how often the magnets may be ramped reliably. Much of the structure in the magnet is metal and is exposed to dramatic changes in magnetic fields. This is especially true in the steel flux return. Large current loops form in these resistive regions and heat the entire magnet. This, in addition to heat leaks, can place a sizable load on the refrigeration systems of an accelerator.

* Reprinted with permission from "Application of Nb3Sn Superconductors in High-Field Accelerator Magnets" by Andries den Ouden, et al., 1997. *IEEE Transactions on Applied Superconductivity*, Vol 7, 733-738. 1997 by IEEE.

3. TAMU SERIES DIPOLE DESIGN

The TAMU version of the block dipole is a series of racetrack windings stacked on top of each other to form a complete package. The top and bottom windings are single-layer windings which are wound around a narrow titanium mandrel. The middle doublet consists of two windings wound around a larger mandrel which houses the region for the beam tube. The middle doublet is open on the ends in an alligator mouth fashion to allow the beam tube to extend from the coil.

The coil loading strategy used by TAMU2 is to use minimize the preload on the conductor itself [21]. The amount of preload is just enough to prevent excess movement and compress the windings sufficiently to get a linear response. Parts of the stress management strategy are also used to carry out this preloading strategy. Other than the minor load on the conductor, all other preloading stressed the internal structure of the coil and not the windings.

3.1. Stress Management

A new strategy that is currently under development in the TAMU series of dipoles is Stress Management. This strategy divides, what would otherwise be a large continuous coil, into multiple windings. Currently, only two windings are used, an inner winding and an outer winding, for each racetrack. The strategy attempts to mechanically decouple the inner and outer windings and thereby transmit the Lorentz loads from the inner winding directly to the supporting steel instead of through the outer winding. Several technologies have been developed to permit this process and the division of coils also has the added advantage which is discussed later. The key components of the stress management strategy are shown in figure 3.1.

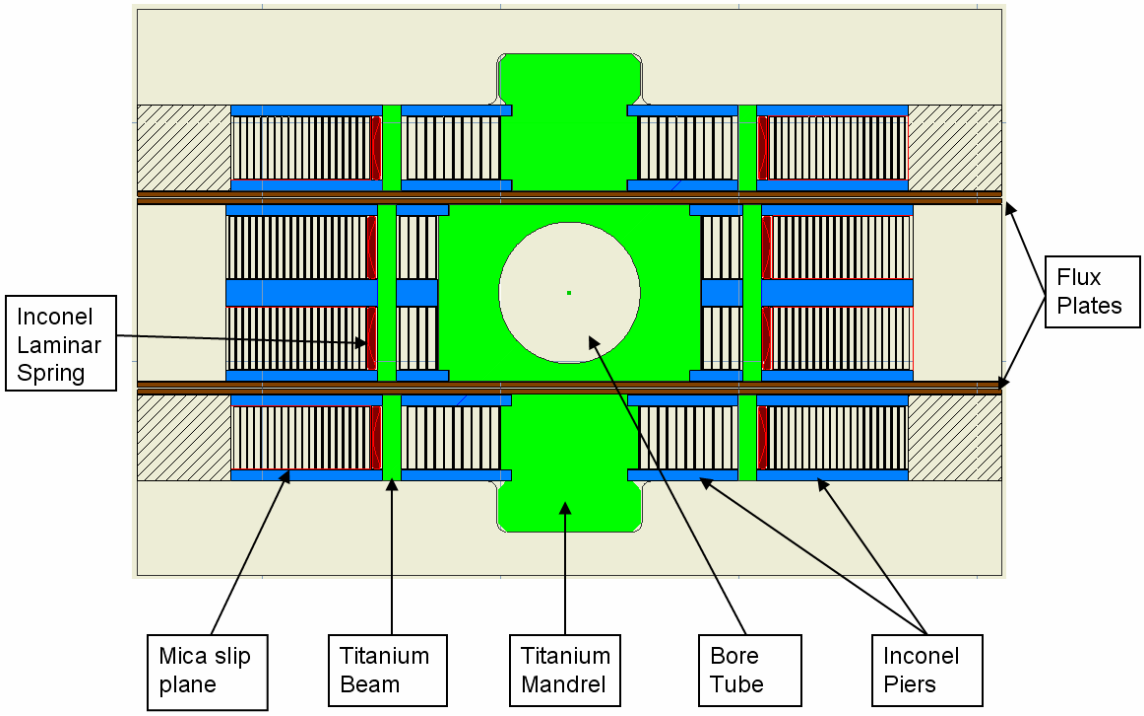

Fig. 3.1. Diagram of TAMU4 with stress management components labeled.

3.1.1. Piers and Beams

The internal support that intercepts the loads in the stress management strategy is the pier and beam structure. The titanium beams divide, what would be a normal coil in a standard block dipole, into an inner and outer winding. The Lorentz load from the inner winding is intercepted by the beam instead of being transmitted it directly to the outer winding. The beam transmits its load to the Inconel piers which further transmit the load to the outlying steel support structure, which is demonstrated in the calculation shown in figure 3.2. In this fashion the loads from the inner winding bypass the outer winding altogether. An analogy would be a two story building. The beam would be the second floor while the piers would be the walls. In this picture, the gravitational load from an object on the second floor rests on the beam which in turn is loaded upon the walls which would be the piers. Just as the gravitational load bypasses any objects on the first floor, the load of the inner winding bypasses the outer winding.

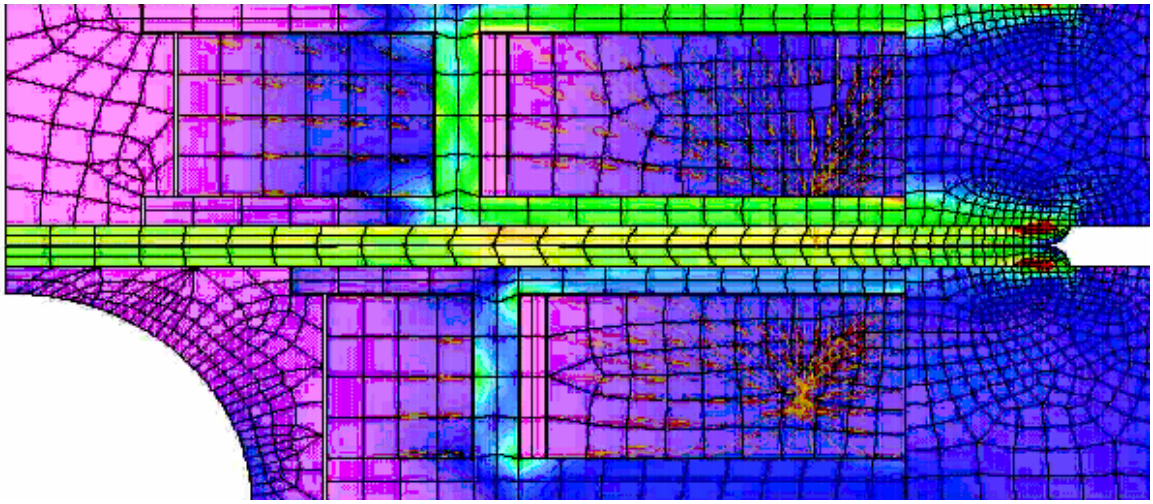

Fig. 3.2. Calculation of the mechanical stresses in TAMU4. High stress regions in green and yellow. Low stress regions are in purple and blue.

3.1.2. Springs

Stress management requires a soft-modulus element to work. No matter how strong the alloys used in the pier and beam structure, they will deflect elastically under the immense Lorentz loads. Without the Inconel springs, shown in figure 3.3, such deflection would cause the stress on the inner winding to partially transmit through the outer winding. In order to enforce transfer of stresses to the support matrix, a laminar spring is located at the inside surface of the outer winding, between it and the beam. The spring absorbs the slight deflection of the support beam without significant loading on the outer winding. This is the first of two very important functions that are both very vital to Stress Management that the springs provide. The second function of the springs is to load the outer winding against the steel support structure. By placing the outer winding in intimate contact with the outlying steel, the outer winding motion is minimized under the loads at high fields as well as insuring the placement of the outer winding.

Fig. 3.3. Fixtures for fabricating springs as well as two straight springs.

3.1.3. Coil Loading

The stress management strategy employs a more effective method for preloading the coil against the surrounding flux return structure. In conventional cos θ dipoles, a preload, ~equal to the maximum Lorentz load expected in operation, is delivered directly to the coil at room temperature (when the preload is first applied). Since the materials of the coil, insulation, and epoxy impregnation have significantly lower yield strength at room temperature than at cryogenic temperature, this preload presents a very real problem for high-field dipole construction.

In contrast, in the TAMU series of block-coil dipoles, the (similarly large) preload is applied to the stress management structure, which is as strong at room temperature as at cryogenic temperature. The preload transferred to the windings inside this structure is determined by the compression of the support structure to the point when all its elements are in hard contact, relative to the compressed thickness of each winding package. The pier lengths are designed to be just enough to compress the laminar springs to the midrange of their travel and to remove the soft-modulus portion from the stress-strain response of the winding package so that it is in a linear response region of compression.

The stress management structure is supported on the inside by the mandrel, figure 3.4. The mandrel is the winding post of the inner winding and is made of a series of titanium laminations. These laminations reduce A/C losses within and thereby reduce the heat load at the high field region of the winding where the conductor is running closest to

its margin. Titanium was chosen for its expansion coefficient which is less than that of the surrounding materials in the winding and has two benefits. During reaction bake, the mandrel expands less than the surrounding parts which gives the inner winding room to "breathe" as it expands and contracts. As the magnet cools to cryogenic temperatures, the mandrel contracts less than the surrounding elements of the stress management structure. The preload delivered during assembly at room temperature is thereby maintained through cool down to cryogenic temperature.

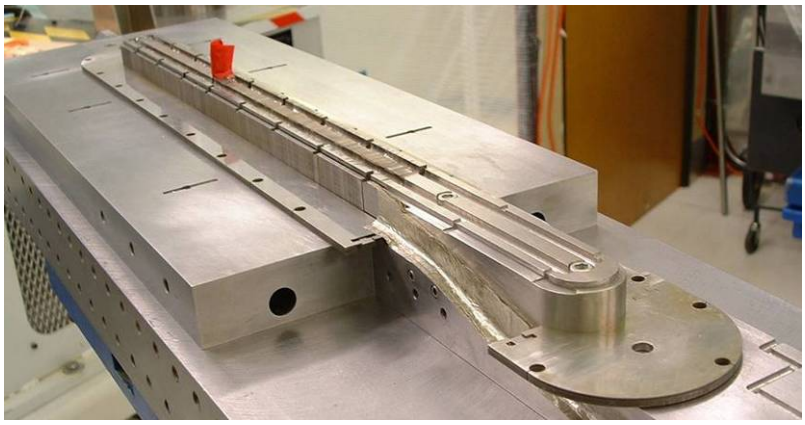

Fig. 3.4. Laminated titanium mandrel. Used as both a winding post and for preloading the pier and beam structure during cool down.

3.1.4. Bladder Preload

External preload comes from the two bladders that are inserted along the sides of the windings. These bladders are inflated to 13.7 MPa at 80 °C. The materials with which the bladders are filled has a net zero coefficient of expansion; so as the coil contracts around the bladders, the load remains constant.

Since the windings are not preloaded directly and are prone to minor movement, the heat released by the movement must be minimized to prevent a stick-slip induced quench. For this reason mica slip planes have been installed along all faces of the winding. mica paper, which was used, does not impregnate with epoxy during the epoxy impregnation process so will release a minimal amount of energy at lower forces. This will greatly reduce the DQ which adiabatically heats the windings. A study was done to determine the force required for release [22].

3.1.5. Friction-Locked Ends

In an effort to reduce the size of the fixtures at the magnet ends, the bladders above and below the windings friction lock the end regions of the coil. The parts at the coil ends have a large surface area and are under vertical load from the bladders. The bladder pressure is set at 4.1 MPa at 80°C. The titanium beam, which separates the inner and outer windings also receives a much greater load from these bladders at low temperatures, shown in figure 3.5, due to its reduced contraction. By friction locking these pieces together and reducing the size of the end fixtures, less length is required in the termination structure of each dipole, resulting in more efficient bending in a collider arc where the dipoles are placed end-to-end.

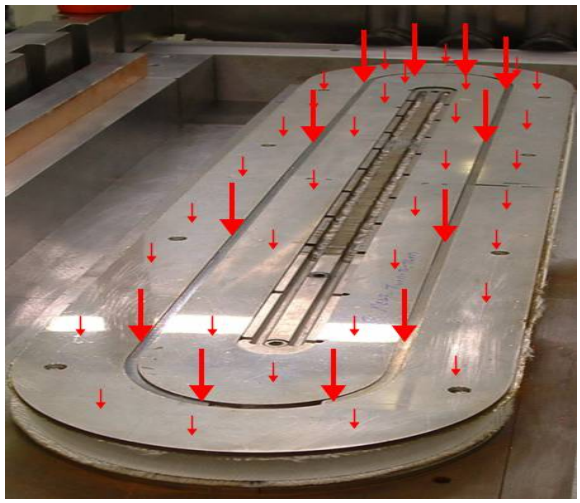

Fig. 3.5. Vertical preload. As the magnet contracts during cool down, the titanium contracts the least. This places much of the vertical load on the titanium which friction locks it into place.

3.1.6. Conductor Grading

A secondary problem with a block dipole is that an individual racetrack coil is exposed to both the high field and low field regions. Because of this, the same high performance conductor must be used in the outer low field regions, where it is not required, as in the inner high field regions. The division of the coils that stress management makes into inner and outer windings neatly solves this problem. The

windings could also be relabeled high field (inner) and low field (outer) windings as it is only the inner winding that is exposed to the high field region. The windings may be fabricated with different conductor just as easily as with the same conductor, which permits the use of a mixed strand conductor or even a different type of conductor for the outer windings.

3.2. Gapping Element

The highest field point in a magnet with a geometry similar to the TAMU series magnets occurs at the very ends of the winding post, if preventative steps not are taken. This will be substantially higher than the high field seen in the straight sections of the conductor and will therefore limit the overall performance of the magnet. To reduce this effect, a gapping element has been introduced during the winding process. It effects have been calculated in figure 3.6. This piece is composed of steel and lies between the third and fourth windings on the ends of the inner winding.

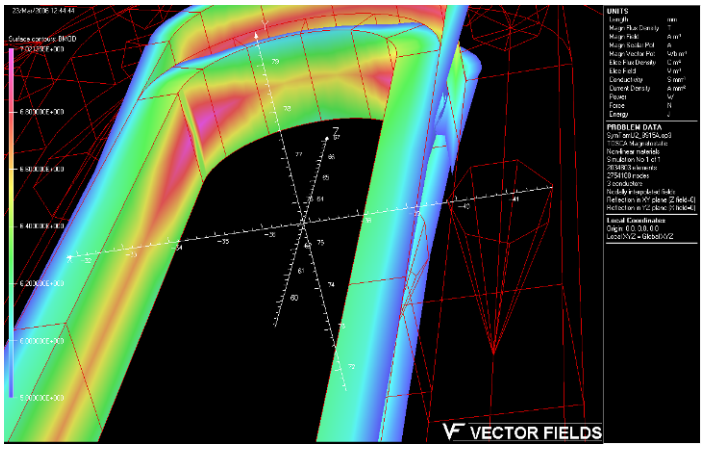

Fig. 3.6. Three dimensional asymmetric calculation of TAMU2. The high field point of the magnet is the pink region.

3.3. Flux Plate

Due to the large effective filament diameter, an accelerator quality Nb3Sn dipole is more challenging to build than a NbTi dipole. There are two challenges that must be overcome before an accelerator quality field is possible. The first is persistent current

multipoles. These depend on the current history of the magnet and are most pronounced at low fields. The second is known as snapback. This phenomena was first observed in the Tevatron during and immediately after loading proton bunches into the main collider ring for acceleration. Once an accelerator has already finished a full cycled of ramp up and down it must load proton bunches for further experiments. During the loading the magnetization in the filaments decays exponentially over time. This is caused by the decay of magnetization effect due to their finite lifetimes. Once the accelerator resumes ramping to high field, the magnetization immediately shifts back to the original curve causing a brief peak in the sextapoles component of the field. Snapback can not be corrected for with other magnets and must be dealt with proper design of the dipole itself.

As both these effects are most disruptive at low fields, they can be reduced by the introduction of a flux plate. This plate is a steel sheet which lies directly above and below the aperture. The steel is unsaturated at the low fields and enforces a dipole boundary condition. This reduces the effects by almost a factor to ten which is demonstrated in figure 3.7.

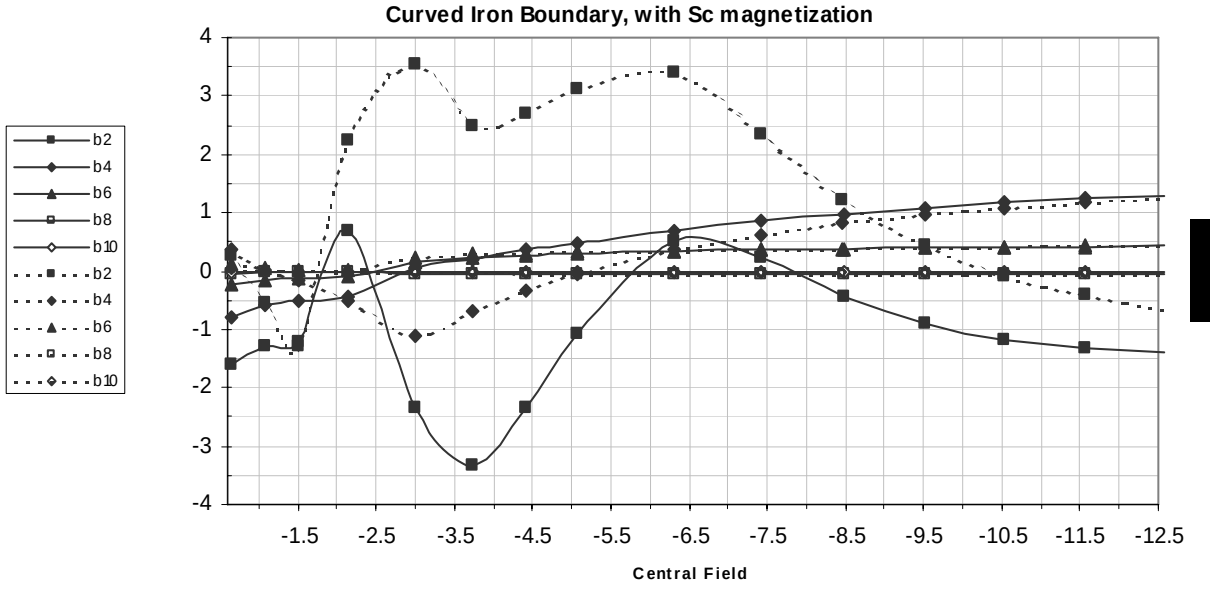

Fig. 3.7. Flux plate effects. Difference in multipole moment strengths with and without the flux plate during a simulated magnet ramp.

4. TAMU2 MAGNET FABRICATION

4.1. ITER 622 Conductor

The conductor used for the fabrication of TAMU2 is ITER 622. Short conductor sections are shown in figure 4.1. This conductor was originally intended for the ITER project which is a magnetic containment fusion experiment. The fusion programs have differing goals from that of an accelerator magnet and so some of the critical parameters of the cable were inferior to a conductor designed for high field accelerator dipoles. Accelerator dipoles tend to ramp more slowly and require a higher current density conductor than what is required of the conductor in the fusion magnets. The ITER conductor was donated to the group free of charge but performs poorly when compared to current dipole conductor. This conductor did meet the requirements of TAMU2, which are rather low for a dipole, since this is the first Nb_3Sn dipole to be built at Texas A&M. TAMU3 and beyond will require high performance conductor.

Fig. 4.1. ITER conductor samples. On these four ITER622 conductor strips the chrome has been etched from the majority of the pieces.

The ITER conductor has been fashioned into a Rutherford configuration with 30 strands. This configuration is very stable mechanically and provides dense packing of the conductor strands. This configuration also eases coil winding and makes for convenient blocks in the block coil dipole geometry.

This conductor uses an internal tin process to create the Nb_3Sn phase. During the reaction bake cycle the tin diffuses into the copper matrix creating bronze. At the final phase of reaction bake the tin then diffuses from the bronze into the niobium. This process can provide for high current densities. However the conductor obtained is rather limited. Its performance ranges from 610-800 A/mm^2 when measured at 12 T and 4.4 K. Due to this process the conductor has a large filament size. While the niobium filaments are very small they tend to cross-link, which forms a much larger effective size, ranging from 50-100μm. Cross sections of the conductor are shown in figure 4.2.

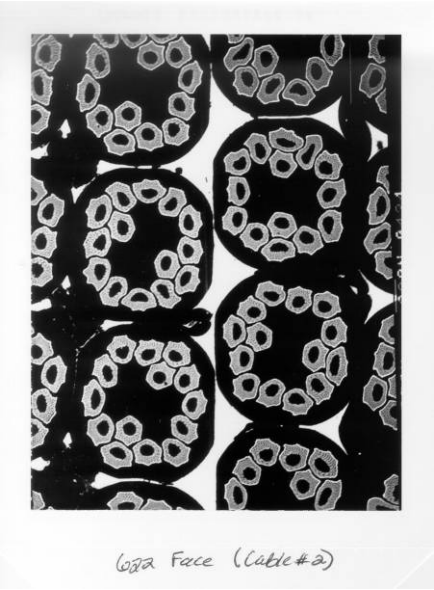

Fig. 4.2. Cross section of ITER622 conductor.

Since this conductor was originally made for fusion research, which requires high ramp rates, the conductor strands were coated with chrome. Chrome has very poor electrical properties and does a significant job electrically isolating strands from each other by increasing the contact electrical resistance. This reduces the size of the inductive current loops that are generated by a changing magnetic field, which in turn reduces the amount of heat generated by these resistive loops.

4.2. Cable Wash

Conductor with S-glass insulation, shown in figure 4.3, ships with a coat of lubricant. This lubricant is needed, because without its, the extremely fragile S-glass would destroy

itself when handled or moved. The lubricant, primarily starch, which was applied by the manufacturer, poses its own problems which must be addressed. One of the components decomposing starch produces during a reaction bake cycle is carbon. Carbon is a semiconductor and will compromise the electrical integrity of the winding, if present. To prevent this, the starch must be removed from the conductor and a different lubricant must be applied in its place. The lubricant of choice to replace the starch is Palmitic acid. This material is chosen because of the components into which it decomposes. These components are all in the gas phase at 340 °C and easily removed with a gas flow during the first phase of the reaction bake cycle.

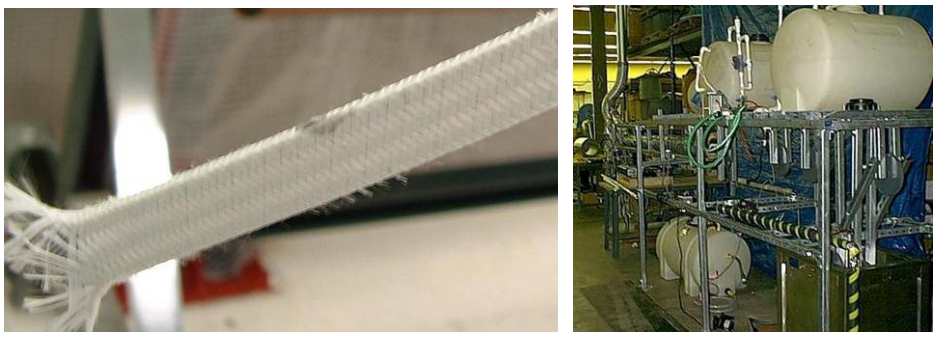

Fig. 4.3 S-glass preparation. S-glass insulation for the conductor on the left and the fixture for washing the S-glass on the right.

A special cable washing fixture was constructed to accomplish this which is also shown in figure 4.3. The cable is run through two ultrasonic bins. The first bin contains Alconox detergent which is circulated from a large premixed reservoir. This first bin washes the starch from the conductor. The second bin has a constant fresh supply of heated reverse osmosis (RO) water which rinses any excess materials and detergents from the conductor. The water is heated to assist the drying of the conductor. The drying is performed with assistance from a hot air fixture. Once the conductor is dry a spray of Palmitic acid is applied to the edges of the conductor only which is shown in figure 4.4. This is done as the handling of the conductor during the winding process is primarily on the edges and also greatly reduces the amount of material to be removed during the

reaction bake process. Once the lubricant is applied the conductor is wound onto another spool at the far end of the cable washing fixture.

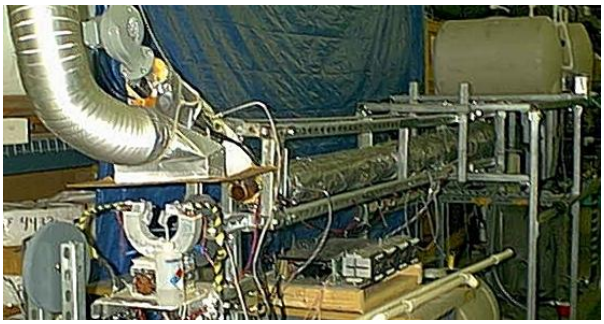

Fig. 4.4. Palmitic acid application. After the cable is dried, Palmitic acid is sprayed onto the edges of the S-glass insulation.

4.3. Ten Stack Test

To determine the mechanical properties of the windings, a ten stack test is performed. These tests determine the mechanical properties of the winding. This information, shown along with a picture of the fixture is shown in figure 4.5. This is crucial to know precisely how much load to place on the winding with shims. The exact size of the windings must also be known so that the leads to each winding can be precisely positioned to the S-transitions into and out of the coil. Ten stack tests were performed at room temperature and at 77 K both with and without springs. The goal was to load the coil just enough to remove the "fluff" which would place the coil in the elastic linear response region.

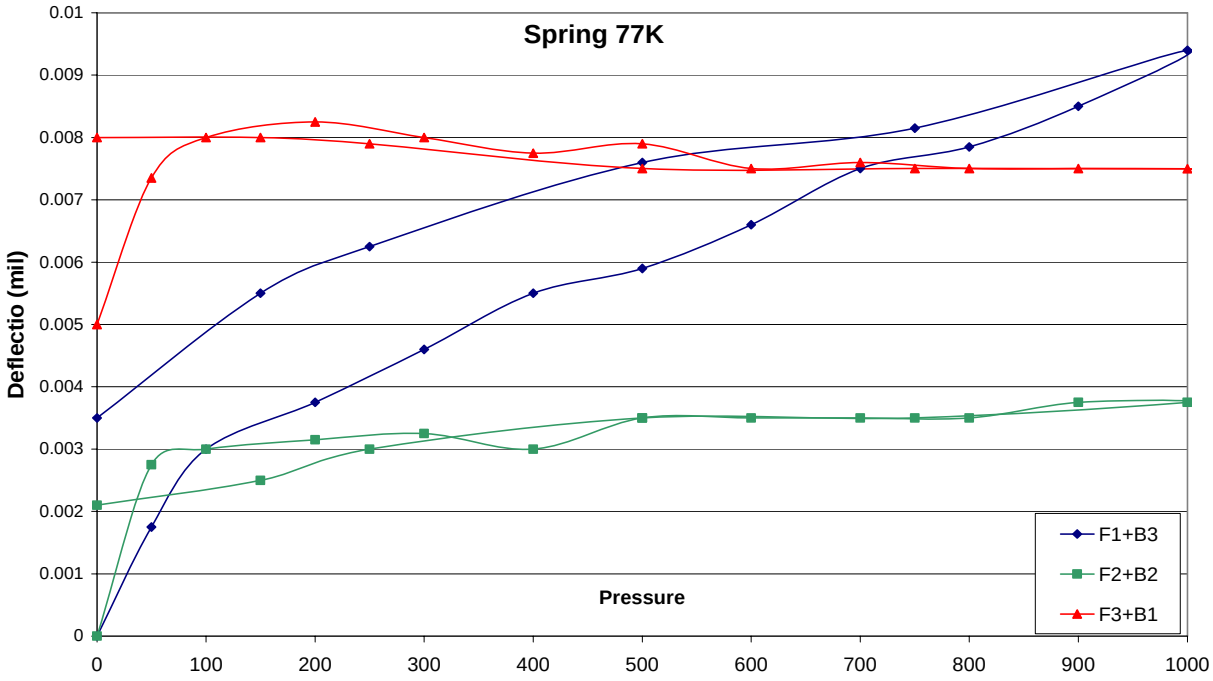

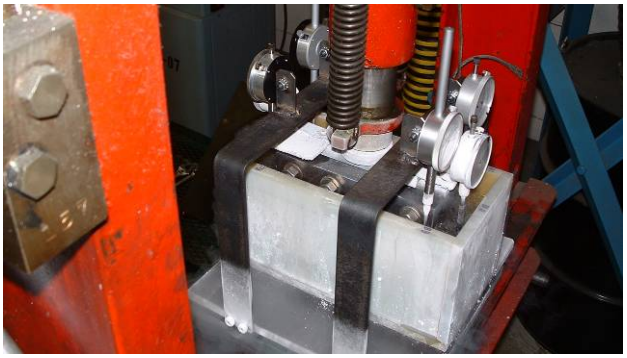

Fig. 4.5. Spring preload. Top: data taken from the ten stack test at 77 K with a spring in the fixture. Bottom: A hydraulic press loads the fixture containing the ten stack and six dial indicators take measurements.

4.4. Coil Winding

Before coil winding can begin, several steps must be taken and parts fabricated. Two crucial pieces to the winding process are the voltage taps and the leaf shims. The voltage taps are carefully cut strips of copper that are ¼" wide and .002" thick. The S-glass, at the points where the taps are to be installed, has slits cut in it and the strips are

inserted. The locations are shown in figure 4.6. The strips weld themselves directly to the copper on the exterior of the conductor during the reaction bake.

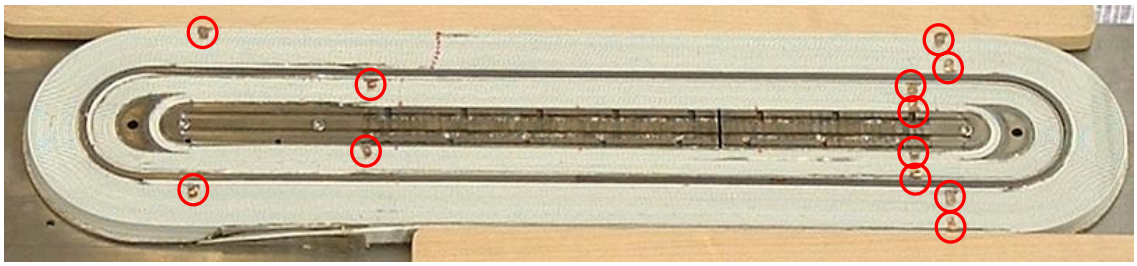

Fig. 4.6. Location of the voltage taps in TAMU2.

The leaf shims are an integral part of the winding process which may only be fabricated once the ten stack tests have been performed. The leaf shims properly load and position the winding so that the conductor lines up precisely with the S-bend transitions for the leads. The leaf shims are laminations of stainless strips that are feathered for a gradual transition and are spot welded together which are shown in figure 4.7. The shim is then placed inside an S-glass sock to protect the conductor and minimize the chance for shorts to the surrounding structure.

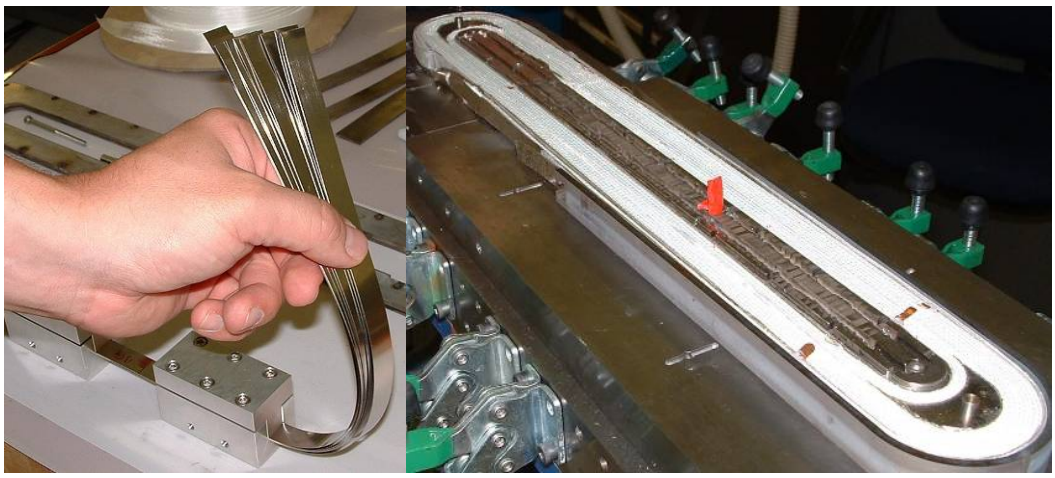

Fig. 4.7. Leaf shims and their locations. Right, leaf shim pieces are being prepared for trimming just prior to welding. Left, location of the leaf shims.

Additional parts needed for coil winding are the S-glass and mica slip planes. These must be accurately cut to allow for the S-bend transitions as well as for the gas and epoxy feed throughs. It was found that flame cutting the pieces with an oxy-acetylene torch, shown in figure 4.8, resulted in much more accurate pieces. These pieces were cut together in packages which bonded the edges together, as seen in figure 4.9, providing a more durable package.

Fig. 4.8. Torch cutting mica. Mica and s-glass are sandwiched between two forms and are cut with a torch.

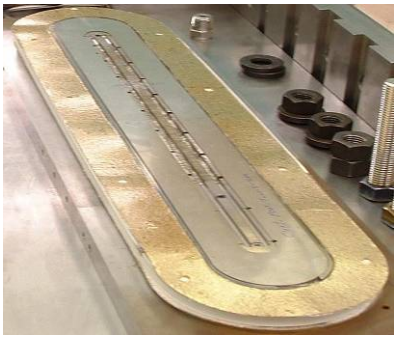

Fig. 4.9. Mica plane installed on top of the outer coil on the left.

All areas of the conductor are well protected from any shorts to case. This is achieved with several layers of mica and S-glass that are crucial to the slip planes but also offer conductor protection and low force release on the region where the conductor could contact the case. The sides of the winding and the S-bends are also well insulated with additional mica and S-glass.

Once the winding and lead packing has been completed the final winding step may commence. The titanium mandrel has one lamination that is designed to be removed

prior to reaction bake shown in figure 4.10 with a red flag attached. This gap allows for contraction of the conductor during the reaction bake. The gap also provided a short for the gas flow and was plugged with RTV to force the gas to flow through the windings.

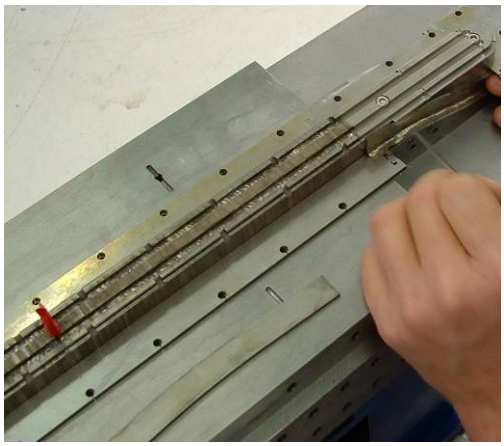

Fig. 4.10. Titanium mandrel just before winding.

4.5. Reaction Bake

Commercial furnaces that are capable of achieving the temperatures needed while controlling the atmosphere inside tend to be in the price range of $100,000. Due to the cost, it was decided that a custom-built furnace would be far more economical as well as possibly achieving superior results. In addition to the initial costs, future upgradeability was also examined. Using commercial units, upgrading to accommodate longer length coils would require the purchase of an entirely new unit, while the custom unit is easily upgradeable by the addition of kiln sections. As a result of both the immediate and as well as the long term benefits, the decision was made to built a furnace in-house.

The furnace consists of 3 main parts. The first is the base plate which is mounted on rails. This piece provides all of the utility ports that are required for the reaction bake process. These ports include gas, thermocouple, and power feed throughs which are shown in figure 4.11. There are a total of fourteen ports for gas flow allowing for the capacity of multiple independent atmospheres inside the furnace during reaction bake. These ports also allow for multiple flow paths through the coil which greatly aids in the removal of vapors from volatilization and decomposition of contaminants within the coil.

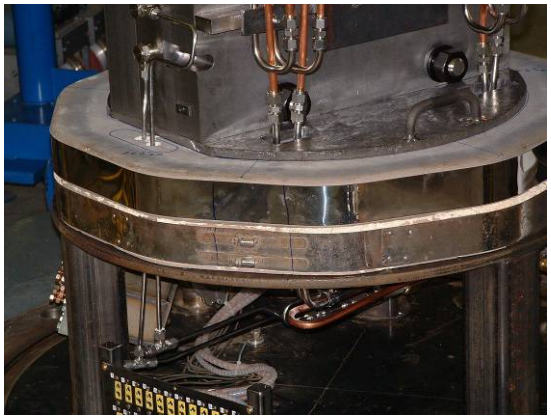

Fig. 4.11. Furnace base with the coffin set on top.

To seal the environment from the outside a large vacuum vessel, which is attached to a crane, is lowered onto the base plate, allowing a low grade vacuum to be drawn on the interior, shown in figure 4.12. This allows for multiple pump and purge cycles with argon to remove as much of the oxygen as possible.

Fig. 4.12. Oven assembled with the jar suspended from the crane.

The interior contains the unit that provide the heat as well as thermal insulation. These parts are common, off the shelf, pottery kiln sections. These kiln sections, two of which are shown in figure 4.13, are made of an extremely porous ceramic brick. These

bricks contain embedded heating elements. This brick shields the rest of the furnace from the high temperatures; this allows for the use of normal wires in the regions external to the heated zone, as well as minimal additional insulation. There are six kiln sections currently in use and these are paired up to provide three zones for heating. Each zone is independently controlled and the furnace has the power to continue operation even if one zone fails completely during the reaction bake process. This furnace is fully capable of temperatures above 1200 C, well above the temperatures needed for reacting Nb_3Sn conductor.

Fig. 4.13. Coffin extraction from the furnace.

The reaction bake cycle used for the ITER 622 conductor consisted of three stages. The first phase of the reaction bake cycle was to diffuse the tin inside the conductor into the surrounding copper. This was done at a temperature of 210 C for 100 hrs. It was critical that the temperature not exceed the melting point of the tin during this phase or the liquid tin could corrode through the diffusion barrier which would produce improperly reacted conductor as well as large regions of bronze. In a worst-case scenario, the liquid tin could cause shorts throughout the coil. In this phase the voids that contribute to the strain sensitivity of Nb_3Sn are formed. During this phase of the run

there was some difficulty with maintaining a constant temperature. Although the oven had been tested with a dummy load, the temperature varied much more dramatically than had been seen before and required manual switching to keep the furnace temperature stable. This was due to a heating zone cross-wiring error and was corrected without interrupting the run. Once fixed, the oven temperature was stable.

The second stage was to remove the Palmitic acid from the conductor insulation. The Palmitic acid was applied during the cable wash to provide for lubrication during the coil winding. The acid decomposes into CO_2 and other gasses and most are removed by the argon gas purge which flows through the coil. This was done at a temperature of 340 C for 48 hrs and was essential for maintaining the electrical integrity of the coil by removing the organics from the coil before proceeding to higher temperatures

During this phase a critical logic flaw was discovered in the Omega temperature controllers. This flaw caused the temperature to overshoot but was dampened by killing power to the furnace until the problem could be understood. An additional measure was taken by greatly increasing the flow of cold argon gas directly to the coil. Once the temperatures had equalized the power was restored to the furnace and the reaction bake continued.

In an attempt to determine the benefits of the edge on Palmitic acid application, the materials, other than the CO_2, removed from the coil were captured. This was done by heating all of the gas feeds out of the coil with a closed cycle hot water system to prevent the material from solidifying in the lines. From the heated lines, the gas was channeled through cool stainless filter cans and then through bubblers. At room temperature the material solidifies and the additional mass in the filter cans was measured. To measure the additional mass for the bubblers, the water was carefully evaporated and the flasks were then weighed.

Table 4.1

Measurement of material removed from coil during reaction bake.

Material Mass **13-Jul-04**

Filter Cans

	Just After Bake	2 Weeks After Bake 7/6/2004	
IL	1254.8	1254.7	0.1
IT	1243.45	1243	0.45
OL	1282.1	1281.6	0.5
OT	1291.1	1291.5	-0.4

Flasks

	With Material Dried 7/12/2004		Cleaned 7/13/2004		Amount of Material	Total	
IL	271.3	-	271.05	=	0.25	0.35	g
IT	271.7	-	271.4	=	0.3	0.75	g
OL	271.1	-	270.5	=	0.6	1.1	g
OT	273.3	-	272.7	=	0.6	1	g

The final phase of the reaction bake cycle was performed at 650 C for 180 hrs. At these temperatures the tin is pulled from the surrounding bronze to form the Nb_3Sn conductor. Stresses in the copper from the cabling process are relieved, which causes each winding to contract slightly. A special lamination in the center of the titanium mandrel is removed just prior to the reaction bake cycle to compensate for this contraction. The entire reaction bake process is shown in figure 4.14.

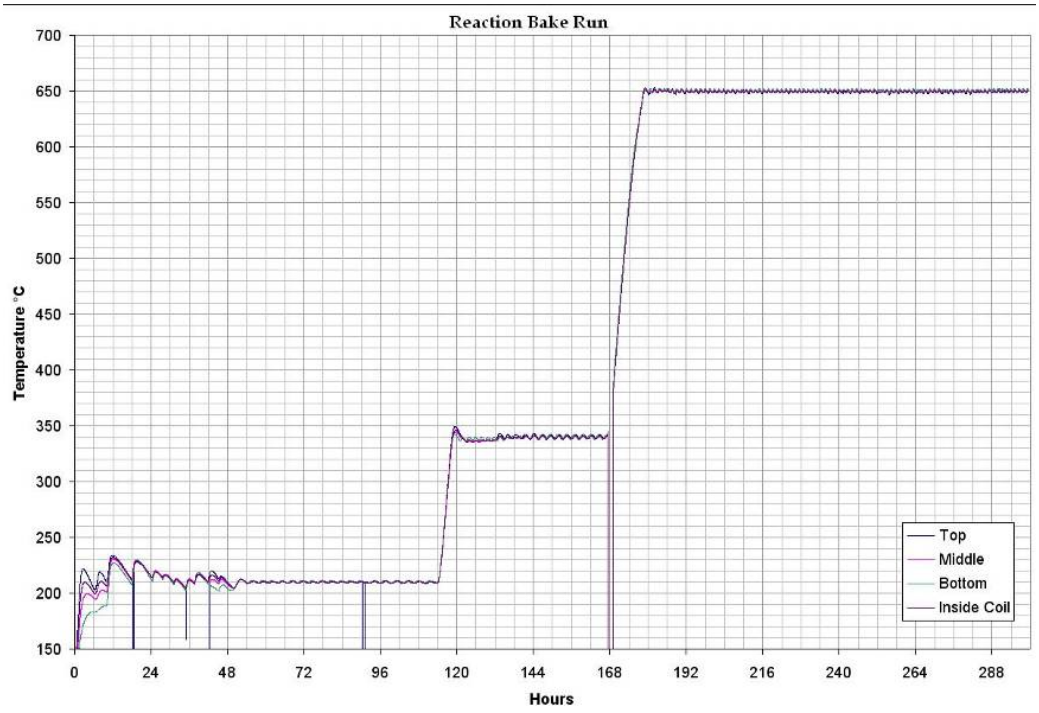

Fig. 4.14. Graph of the total reaction bake cycle.

Once the reaction bake cycle was completed, the coffin was opened and the coil was examined. Initial examination revealed that the keys which lock the stainless piers together, as seen in figure 4.15, had been forcibly pulled apart. After many careful measurements, it was discovered that the titanium had changed dimension which stressed parts of the stress management structure. Later dilatometry tests from coupons cut from the same plate at the titanium in the coil showed that the titanium underwent substantial dimension change through a reaction bake cycle.

Fig. 4.15. Pier damage just after reaction bake.

Another post reaction bake discovery concerned the gap from the removed mandrel lamination. RTV was used to prevent a gas flow short during the 210 °C phase of the reaction bake cycle. Previous tests had shown that RTV becomes an extremely brittle substance at reaction bake temperatures even when mildly confined. The RTV in the gap did not behave as the tests had shown and compressed into a dense material, shown in figure 4.16. As a result the gap remained slightly open after reaction bake.

Fig. 4.16. RTV jammed in the gap of the mandrel.

4.6. Splicing

The leads of the coil, after reaction bake are extremely brittle and prone to accidental damage. For this reason, it is necessary to splice the leads to pieces of NbTi cable which are far more capable of withstanding mechanical stresses. All splicing is done in low field regions and on the same end of the coil so the NbTi can handle the current loads required. The leads emerge from the thick skin, which contains the S-bend transition regions, into a set of protective steel extension blocks. The goal of this entire process was to minimize any chance of strain degradation in the leads while still providing power for the magnet.

Before the splicing could begin with TAMU2, the chrome coating on the ITER 622 cable had to be removed. Chemically etching the chrome with Muriatic acid provided the best results as it removed the chrome on the interior of the Rutherford cable as well as the exterior. Due to the critical nature of the splices, the acid etch was used, although this would later produce electrical problems by damaging the coils electrical integrity. Tests

had shown that the Muriatic acid would not wick up the leads into the magnet. The rinse water, which was not tested, was capable of wicking into the coil and during the etching of the lead, water flushed some acid into the winding. The winding was immediately placed into a vacuum chamber to extract the water as quickly as possible. Nothing could be done about the acid residue left inside the winding. This step was performed prior to reaction bake as the leads were not in the fragile reacted state at this point.

Prior to splicing, the NbTi cable pieces had to be prepared as follows. A special fixture soldered parts of a copper box, that would surround the junction, to the NbTi strips. The fixture also insured that the NbTi strip was filled with solder so that a minimal amount of solder would be required when splicing.

Once the leads had been carefully cleaned they were spliced to the NbTi strips. Two NbTi strips were spliced to each lead to minimize the splice length needed to keep the junction resistance down. The leads were kept inside the protective steel blocks during much of the process. Once the splicing was complete, the joint was surrounded by a G-10 box and wrapped in Kapton. The area was then packed with S-glass for reinforcement during epoxy impregnation. The final step was to weld the protective blocks to the thick skin which permanently attached them to the coil. The steps are shown in figure 4.17.

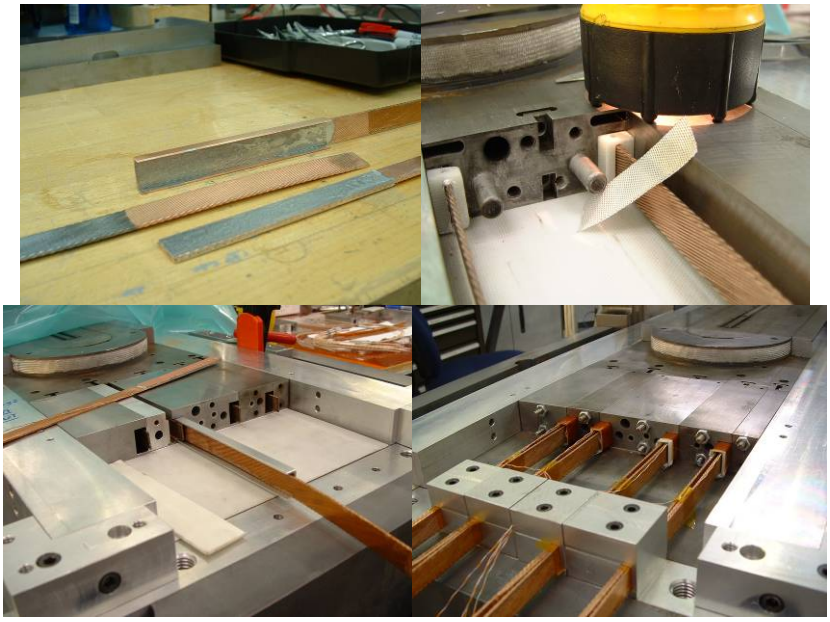

Fig. 4.17. Splicing steps. Top left, Nb3Sn cable with chrome etched and two NbTi pieces complete with attached copper box. Top right, Nb3Sn leads being cleaned and prepared for splicing. Bottom left, NbTi being spiced to the coil leads. Bottom right, all splice junctions completed.

4.7. Ground Plane Installation

In order to properly protect the magnet and measure data from it, multiple fixtures and instruments must be installed. These parts contain materials that can not withstand the high temperatures required during the reaction bake cycle and therefore must be installed afterwards. This includes protection heaters, wire traces, capacitive pressure transducers, and carbon resistors. The protection heaters consist of a copper foil surrounded by kapton for electrical insulation. The heaters are placed directly on top of the windings and are in contact with every winding, shown in figure 4.18. This is to ensure an even quench process which reduces hot spots in the windings as the coil energy is dumped. The traces for the voltage taps are also found inside the kapton which contains the protection heaters. Carbon resistors are installed in the coil to measure very low temperatures.

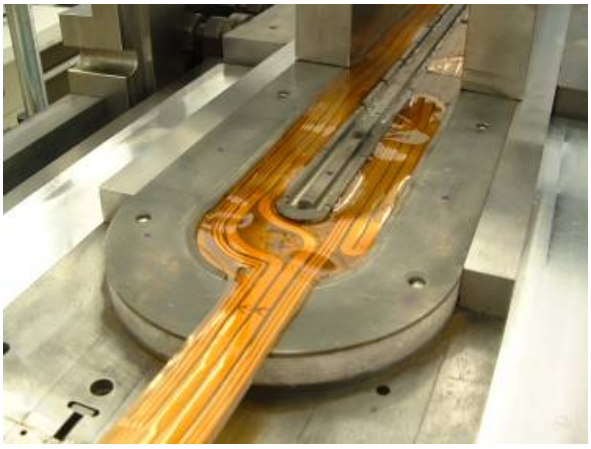

Fig. 4.18. Installation of the protection heaters and voltage tap traces.

Along the outside of the coil are the capacitive pressure transducers, shown in figure 4.19. These measure the load that the outer winding exerts on the supporting steel. It is with these devices that the degree of stress decoupling can be measured. The transducers are seven layers of 0.5 mil stainless steel foil with 1 mil kapton between the foils. The package is capped on top and bottom with a 2 mil kapton layer and bonded together with M-bond 610. This creates a parallel plate capacitor in the nano-Farad range with a soft insulating dielectric. As pressure is applied, the gap between the foils is reduced which raises the capacitance.

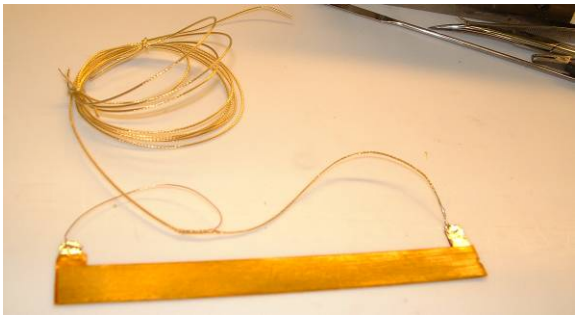

Fig. 4.19. Capacitive pressure transducer.

4.8. Epoxy Impregnation

Due to its brittle nature, Nb_3Sn must be completely supported when placed under mechanical loads. For this reason, coils are commonly vacuum impregnated with epoxy. During the winding and splicing processes, all visible voids are filled with S-glass. S-glass wicks the epoxy extremely well and acts as a fiber reinforcement for the epoxy, similar to reinforced concrete. The resulting package is extremely mechanically robust and durable, a necessity for the high Lorentz loads that are applied when the magnet is energized.

To facilitate this process, substantial development went into the existing epoxy impregnation fixture, shown in figure 4.20. The vessel which provides for the atmosphere control on the fixture is horizontal. It is on tracks and rolls around the coffin, while at the same time supporting it, to mate with the face plate. The vessel contains multiple view ports, internal lighting and a series of mirrors for monitoring the impregnation process.

The face plate, which provides the sealing surface, also contains the feed throughs for epoxy, vacuum, and gas flow. The coffin is fixed to the face plate with a spacer bar for proper positioning, although the face plate does not support the gravitational load of the coffin. This fixture allows for multiple epoxy flow paths, thus minimizing the chance for problems during impregnation. The coil may be rapidly accessed during impregnation if complications should arise. This was the case with TAMU1 in which a minor oversight had to be corrected for proper impregnation.

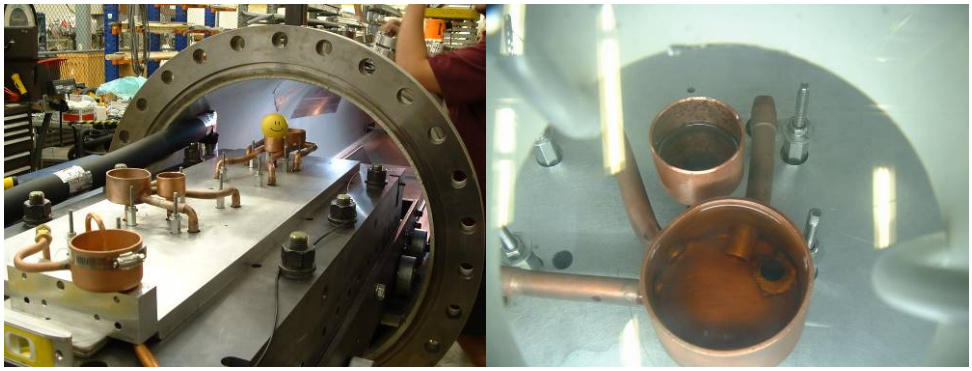

Fig. 4.20. Vacuum impregnation. Left, insertion of the magnet into the impregnation vessel. Right, epoxy cups filled as vacuum impregnation finishes.

4.9. Final Loading

The fashion in which the bladders are used is unique and provides two benefits. The stainless steel bladders ,shown in figure 4.21, perform the function of a smart variable shim which drives down costs on parts by relaxing dimensional tolerances. Most of the tight tolerances required by other magnets are not for field quality but for coil loading. These tolerances are allowed to be loosened with the use of the bladders. These bladders are pressurized with a low temperature melt alloy in the liquid phase commonly known as Wood's metal. The variable interface between the bladders and coil package provides an even hydraulic preload of the coil structure and the Wood's metal, once it freezes, locks the preload in. This is accomplished with the use of the interior bladders which conform to any imperfection that may exist on both the exterior of the coil and on the mating regions of the steel flux returns. This eliminates any potential stress concentrations or gaps that could allow for a loss of preload on the coil package. Two radial bladders are positioned between the aluminum stress tube and the flux return pieces which provide a hydraulic interface, relaxing tolerances there as well.

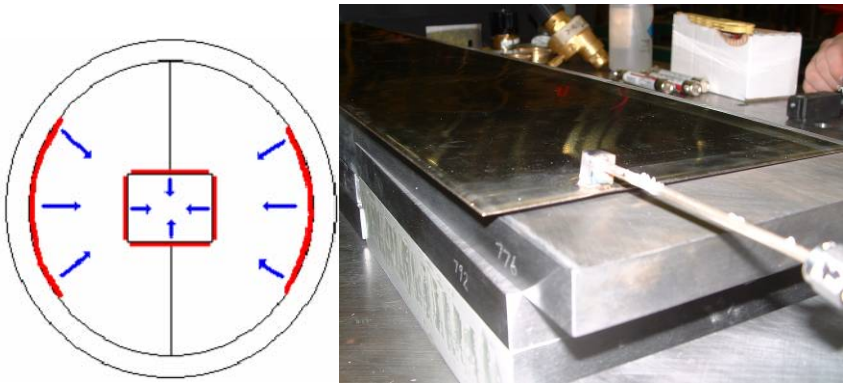

Fig. 4.21. Bladder preload. Right, bladder locations in red. Left, stainless steel bladder.

The particular Wood's metal alloy used was Cerolow-147. This alloy has a melt temperature of 147° F and a unique coefficient of expansion. The net expansion from solidification to 4.4 K is zero. As the magnet pieces contract during the cool down the bladders retain their initial dimension which provides an even greater preload on the coil structure and stress tube.

During the final loading and bladder pressurization process, several pieces need to be assembled to make the final magnet. On the outside is the aluminum stress tube. This is made from a special alloy that does not undergo any brittle phase transitions during cool down to cryogenic temperatures. This cylinder is what ultimately holds the entire magnet together, acting as a large elastic band that holds the flux return pieces together with more force than they will see when the magnet is energized to high fields.

The flux return pieces that are held by the Aluminum Stress Tube are each a series of carefully machined laminations of steel. These laminations were assembled on an accurate steel table and held together with a nitronic-40 rod, shown in figure 4.22. This rod then had a hydraulic piston attached and was strain hardened. The locking nut was then retightened locking the lamination stacks under immense loading. These lamination stacks could, from then on, be moves as a single solid piece.

Fig. 4.22 Steel lamination assembly. The steel laminations are assembled on a table just before the nitronic-40 rods are stress hardened.

The stress tube was then oriented in a vertical position and the two flux return pieces were lowered into the cylinder with the aid of an overhead crane, shown in figure 4.23. Once in position, stainless bladders were inserted between the cylinder and the flux return pieces. The assembly was then heated using a circulating hot water system and heat exchangers that were attached to the sides of the cylinder. Once 80°C was reached, Wood's metal was injected into the bladders which inflated like balloons, providing an even hydraulic interface between the flux return pieces and the Aluminum Stress Tube. The initial length of the lines of the pressurization circuit were heated with hot water jackets. From the end of the water jackets up to the bladders, rope heaters provided the necessary heat to prevent the metal from solidifying inside the lines. It was discovered that accurate temperature control of the rope heaters was very difficult. As a result, it was decided to use water jackets for the complete length of the pressurization circuits. The remaining bladder stems were heated by an aluminum block with cartridge heaters. Each heater was independently controlled with a temperature controller. These changes worked very well in preventing any solidification of the Wood's metal during pressurization.

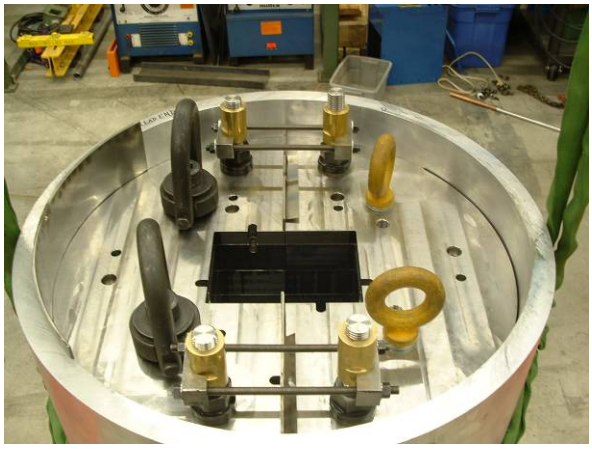

Fig. 4.23. Flux return halves are installed in a vertical position into the cylinder.

Once the cylinder and flux return had been pressurized, the assembly was tilted to the horizontal position. The coil and magnetic mirror pieces were inserted along with four bladders, G-10 sheets, and a wrap of Kapton. Figure 4.24 shows all six bladders attached to their respective circuits. Due to the viscosity of the Wood's metal the bladders did not inflate evenly. This caused the lead end of the coil to raise up which applied torque to the weld point where the stem meets the bladder. The weld broke and the bladder ruptured. To solve this, small loops were installed in the circuits near the bladders which would prevent torque on the weld joints of the bladders. While the inner bladders were being pressurized, pressure was maintained on the radial bladders. The second attempt to inflate the inner bladders was completely successful.

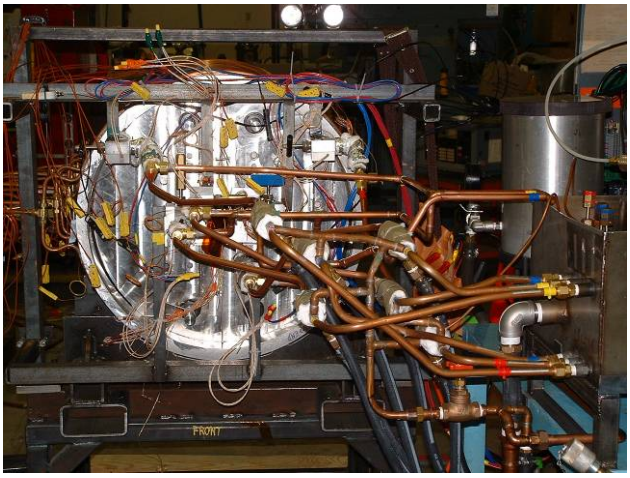

Fig. 4.24. Pressurization of the bladders with the coil and magnetic mirror installed.

During tests it was found that the Woods metal would form large grains if cooled too quickly and potentially critical voids could form inside the bladders. The opened bladder is shown in figure 4.25 with the grains visible on the left hand side. To prevent this, a procedure was developed which would cool the magnet in a carefully controlled fashion. The magnet was divided into four zones. Each zone was connected to a manifold which could be heated or cooled as necessary, shown in figure 4.26. The tail end zone, which was farthest from the point of injection, was cooled initially. All water to the middle two zones was shut off and the zone nearest the lead end was left with circulating hot water. Later, cold water was applied to the middle two zones as well and the lead end water supply was shut off. In this manner a solidification wave passed through the magnet from tail to lead end. During the solidification, pressure was maintained on the bladders to fill any voids as they might happen to form.

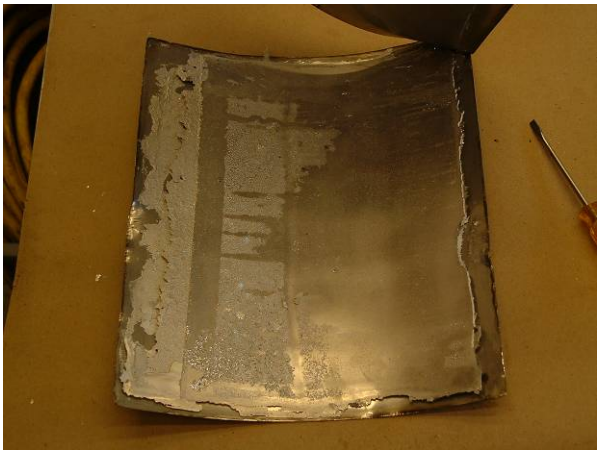

Fig. 4.25. Large grains are formed when the Woods metal is cooled too quickly.

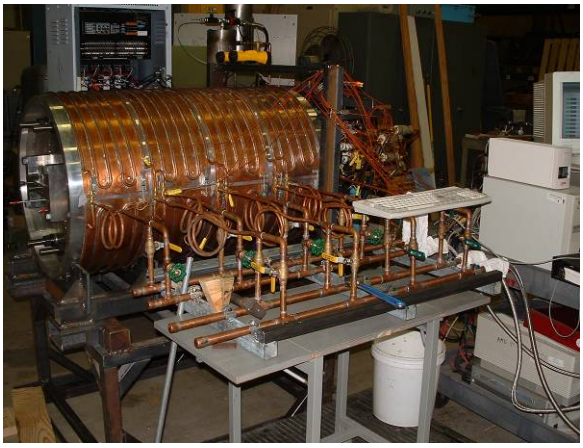

Fig. 4.26. Hot water manifold. Manifold used to carefully control the temperature of the magnet during bladder pressurization.

To load the ends of the magnet, large H-shaped bars were attached to the steel flux returns on both ends. The H-bars contained threaded holes for hardened studs to be inserted, which loaded the ends of the winding directly. Each end used four studs and various strain gages were attached to measure the change in loading during the quench tests. Two of these gages are visible in figure 4.27.

Fig. 4.27. Bolt strain gauges on the ends of the magnet.

4.10. Instrumentation

During a test of a magnet, many variables must be monitored to validate the fabrication and design features. These variables are in addition to any unique technologies that might be examined during the test of a magnet. TAMU2 included many methods for examining the various operating parameters so that accurate data could be acquired.

The voltage taps are the most important for preventing damage to the magnet or the test facility equipment. These are vital for determining if a spontaneous quench is occurring inside the coil. This detection is critical to prevent thermal damage to the coil. A rapid detection also prevents high voltages from being generated which could be damaging to the testing equipment. The quench location and velocity may also be determined from the voltage tap data. The voltage taps are also used to determine the resistance of the splices. Multiple tests were performed on the voltage taps to verify the status of the coil. At room temperatures, turn to turn shorts can be found inside the coil.

To measure the side Lorentz loads, capacitive pressure transducers were installed along the outside of the outer winding. Two transducers were placed along the straight regions while one was placed on the curved lead end of the winding. The transducers were calibrated in a horizontal hydraulic press.

Verification of friction lock was performed by strain gages on the fixtures at the ends of the winding. Four hardened bolts, each with strain gage, were attached to an external

fixture at the ends of the coil. The bolts are torqued to apply a controlled axial load on the coil to prevent the end region from moving under any portion of axial Lorentz stress that was not friction-locked. The strain gages were to measure any change of load during the test run of the coil. Of the four gauges on each end of the coil, two of the gages were full bridges while the other two were a pair of half bridges. The full bridges had the capability of much finer measurement but were wired incorrectly. This brought their sensitivity to that of the half bridges. The strain gages on the bolts were calibrated in the same press at was used for the pressure transducers.

Several electrical checks were performed on the magnet to determine its status throughout the fabrication process. In order to test the voltage limit of coil insulation, the coil was connected to a current-limited high voltage source and the voltage was increased gradually until ~μA leakage current was detected (a high-pot test). The high-pot test was performed on the magnet to determine the maximum voltage that can be permitted to occur during the transients that occur during quench. A lower voltage breakdown requires the quench detection to be more aggressive in initiating the firing of the quench heaters that force the propagation of a quench after it is detected. The allowed time can be dramatically reduced. The voltage breakdown was found to be fairly low, near 200V.

Another electrical issue appeared after the chrome stripping of the leads. The acid which was washed into the coil caused high resistance shorts inside the coil. Earlier in the fabrication, the coils had measured many MΩs to ground; after the vacuum chamber had removed the moisture, the inner coil had a 2 kΩ short and the outer winding had a 20 kΩ short. It was determined that these shorts would most likely increase as the magnet cooled and so the fabrication process proceeded. The electrical issues are shown in figure 4.28.

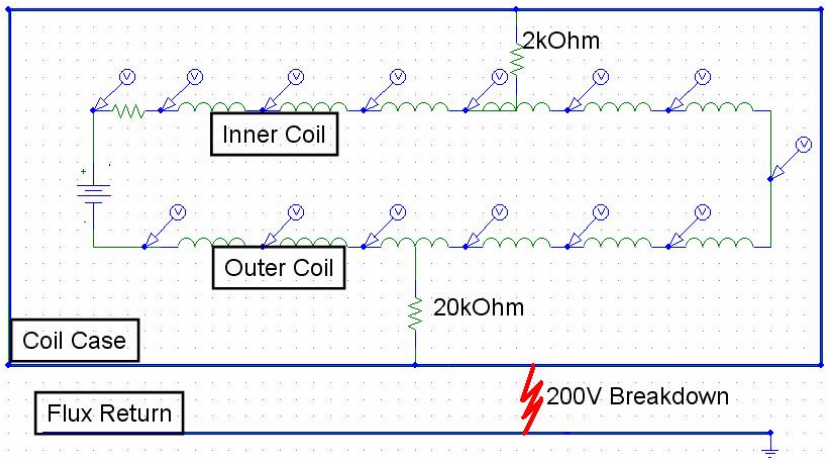

Fig. 4.28. Electrical problems with the coil at 300 K.

4.11. Setup for Testing at Lawrence Berkeley National Lab

Before testing could begin, a series of electrical checks and tests had to be performed at room temperature, during cool down, and at 4.4 K. These checks were taken so that accurate data could be taken during the test and a quench protection strategy could be finalized.

In order to record data from the magnet, signals had to pass through multiple connections and the proper amplifier. All of these connections had to be verified multiple times for both data integrity and to protect the instruments. There were four data acquisition systems in use during the test and each operated on different time scales and measured different parameters.

To measure the pressure transducers, the ramp was paused at a preset current level and the capacitances were measured by a stand alone computer system. The ramp scanner measured on the order of a second. This system measured magnet and cryostat temperatures as well as the bolt strain gages on the ends of the magnet. The 8212 was responsible for measurement of the voltage taps. This unit had a time resolution of .2 ms with enough memory for a 200 ms window. The recorded data from the 8212 spanned the magnet quench with 100 ms before and after the quench trigger. The highest speed unit, the 6810, was not in operation during the TAMU2 test. This device is normally used to track minor coil movements throughout the test.

As the temperature inside the cryostat is reduced and reaches temperatures below 100 K, the resistance of the pure copper in the conductor begins to drop dramatically. The reduction in resistance will approach a finite resistance value, which depends on the purity of the metal, at very low temperatures. The ratio of the conductor resistance at 273 K to the resistance of the final value at very low temperatures is known as the residual resistance ratio (RRR). The conductor for TAMU2 had a RRR of 127.

A high RRR is important for stability when the magnet is operating. While at high field, the conductor is operating close to its performance envelope. Micro-quenches will often occur and some of the current will be shunted through the copper near the micro-quench location. A low resistance of the copper will minimize the thermal energy added to the location and increase the chance that the heat can be conducted away from the region rapidly.

Once at 4.2 K, a high-pot test was performed so that a quench protection strategy could be finalized. During a quench and subsequent energy extraction, high voltages can be generated and an electrical breakdown to ground could damage the magnet and possibly the test facility as well. With a the low voltage breakdown value the coil had at 300 K, the time span for taking at a quench would be reduced as the protection heaters would have to be fired quickly. Also, the stored magnetic energy in the coil would have to be converted into heat within the coil as it became resistive. With a high voltage breakdown, the protection heater timing could be delay and some of the stored energy could be diverted into a resistor bank. Once at 4.2 K the voltage breakdown of TAMU2 increased beyond 600 V. This value was sufficiently high enough.

Before TAMU2 could be ramped to full field, the protection heaters had to be tested. This was done in a series of four trial quenches. The first three quenches were manually tripped at 4 kA. This relatively low current was chosen as the conductor has a large amount of margin and will take a significant amount of heat to quench at these levels. It was during the fourth trial run when the Hall probe was rotated to maximize the magnetic flux passing through it.

A quench is detected by monitoring the balance between the inner and outer coils. This greatly reduces the chance that electrical noise could trigger a false quench. Once

the voltage imbalance crosses a predetermined threshold, the quench protection procedure begins automatically. Once the quench is detected the power supply stops providing current to the magnet. Next, a 15 ms time lapse is allowed for the quench to propagate. The quench heaters are then fired to drive the magnet normal in an even and controlled fashion. This prevents too much energy from being deposited in any region. An adiabatic increase in temperature of the heaters to 100 K was sufficient to protect TAMU2. The final step of switching the current to a resistor bank occurs at 40 ms after the quench is detected.

5. TESTS AND RESULTS

5.1. Training Curve

A series of ten quench runs were performed during the testing of TAMU2 and showed no training what so ever. The ramp rates were low, on the order of 5-20 A/s, to prevent A/C losses from affecting the quench current, which fell in a narrow band about 60 A wide. It should be noted that other non-cosine-theta dipoles have been built with ITER 622 conductor for operation at similar field strengths which showed a very minimal training curve.

Once a quench occurs, a substantial amount of information can be gained by how the quench propagates. Of greatest interest, is the location of the quench. If the conductor quenches in the high field region like TAMU2 did, then the magnet was operating at close to the short sample limit. A quench in a lower field region could indicate damage to the conductor or a possible fabrication error.

As the location of the quench heats resistively, the regions of the conductor in close proximity warm and quench as well. In this fashion, the normal region of the conductor will expand and travel down the length of the conductor. The velocity at which quench propagates yields additional information on how close to the limit of performance the conductor was operating at. A high velocity indicates very little remaining margin left remaining. The quench velocity for TAMU2 was on the order of 16 m/s which indicates that the conductor was closer to 90% of the short sample limit.

The dominant direction of quench propagation is one dimensional and down the length of the conductor; given time, enough heat can diffuse through the insulation and quench adjacent windings. The pattern of diffusion of heat through the insulation is much slower than the quench velocity because the glass and epoxy are thermal insulators as well as having a vastly higher heat capacity than the conductor. The time from the initial quench until the adjacent winding quenches is a cross check on the packing fraction of the coil. It is important that there is enough insulation to prevent any turn to turn shorts in the coil, however, the amount of insulation must be minimized. The insulation occupies a critical volume which can not carry any current and will reduce the

total number of amp turns in a design for a given volume. A sample quench, during the fourth run, is shown in figure 5.1.

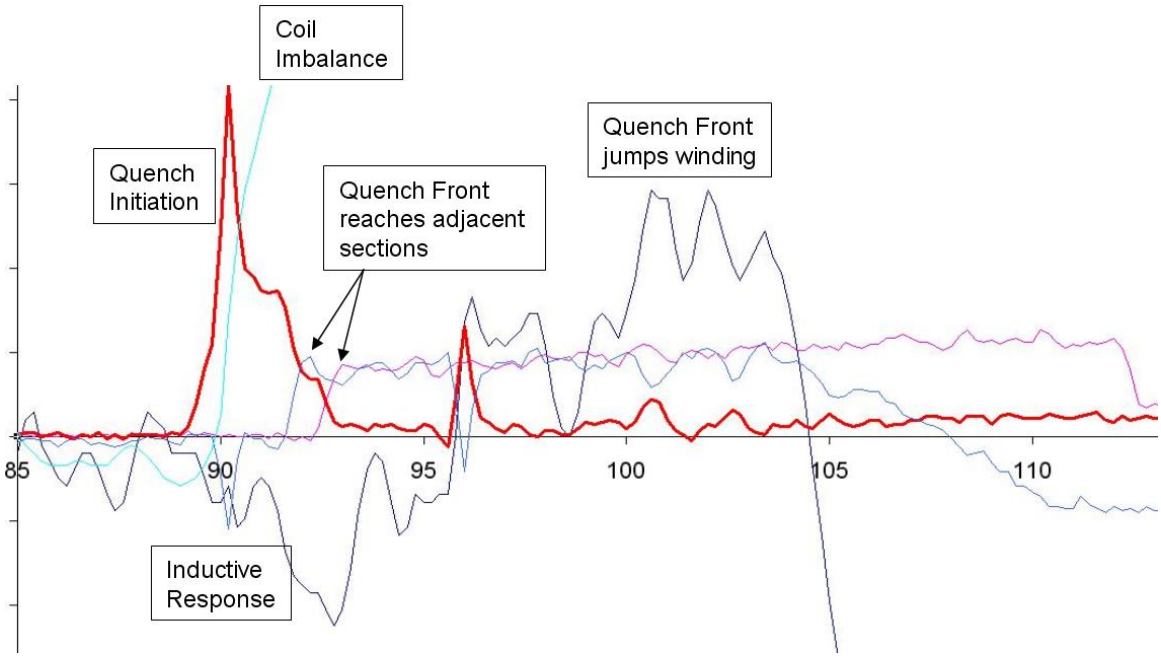

Fig. 5.1. Graph of time (ms) versus the rate of change of the voltage during quench test four.

Two of the quench runs did face issues which don't represent the performance of the magnet. Run number seven simply had a loss of data on the current channel so the instruments were rewired to avoid problems of data loss. Quench run number two was the more dramatic of the two. A stainless steel bolt, which was later to be found magnetic, was left under the bus bars that supplied current to the magnet. At 8030 A the field from the current in the bus bars was strong enough to draw the bolt from the ground into contact with both bus bars. The computer detected a sudden minor voltage change and initiated a quench of the magnet. A summary of the peak current reached for all of the test runs is shown in figure 5.2.

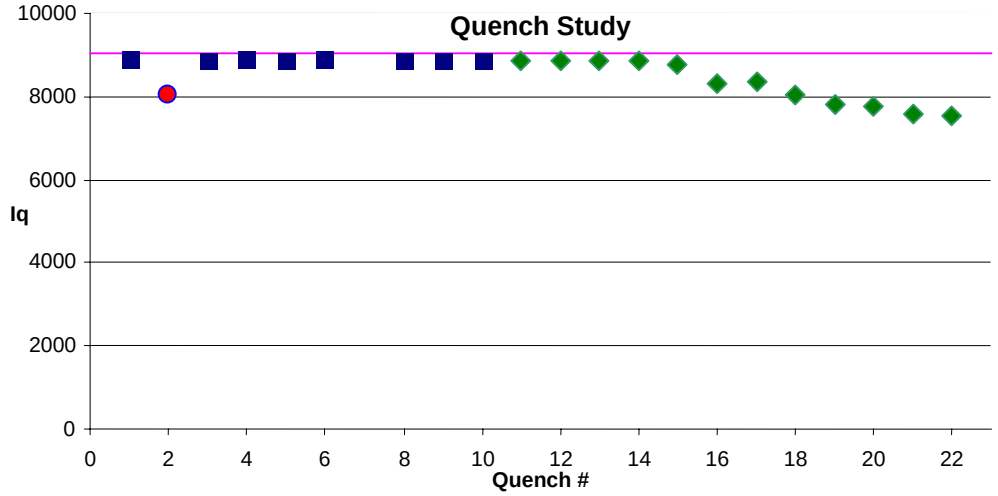

Fig. 5.2. TAMU2 quench history. Quench tests are the blue squares while the green diamonds are the ramp rate study. The red circle was a power supply fault.

5.2. Quench Location

As the flat training curve would indicate, the quenches in TAMU2 were extremely repeatable. The data from the eight successful training runs were very similar to each other. The primary difference in the graphs of the data were the electrical noise. This shows that the magnet quenched in the same location every time, shown in figure 5.3. This point is very near the high field point of the magnet.

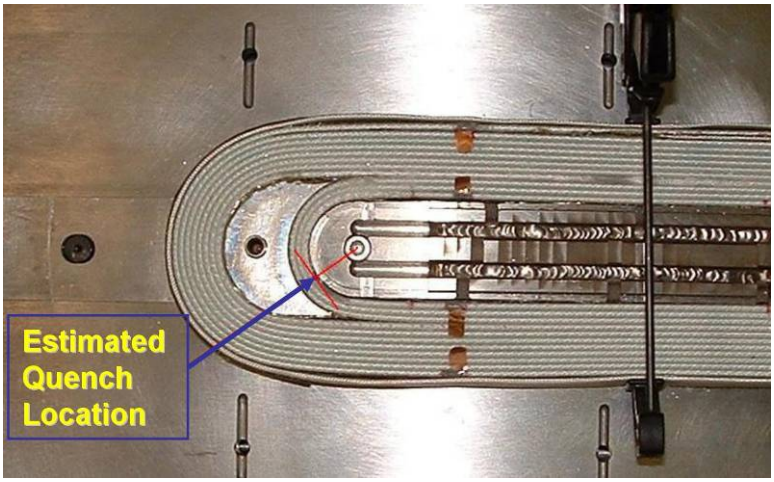

Fig. 5.3. Location where the spontaneous quench began during the standard quench tests.

5.3. Field Strength

TAMU2 reached a field strength of 4.6 T as measured by the Hall probe. As calculated, this would indicate that the high field point in the windings was considerably higher (approximately 6.7 T). Due to the wide performance band of ITER622 conductor, it is difficult to directly determine the fraction of short sample that TAMU2 attained.

Under normal circumstances, a witness sample is included with the coil during the reaction bake process. For TAMU2 this was impractical, as the coil was surrounded by a large steel structure, which caused a considerable delay of the temperature change of the coil. Any witness sample included in the furnace would have received a completely different reaction bake cycle than the coil.

However, it can be indirectly inferred that the conductor used for TAMU2 performed at the high end of its range. This inference can be determined from the quench propagation velocities. The velocities were fairly slow, which indicated that the conductor still had a significant margin remaining as it quenched. This places the performance of TAMU2 at a minimum of 92% of cable short sample. The short sample limit can be seen from the data presented in figure 5.4.

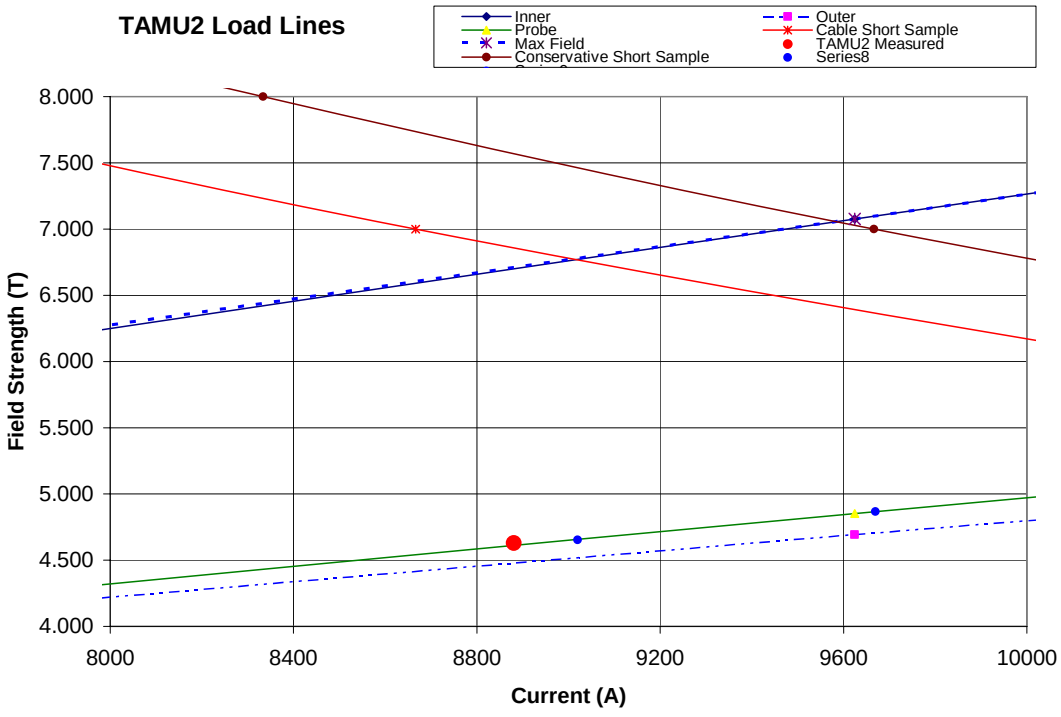

Fig. 5.4. Load line graph for TAMU2.

5.4. Ramp Rate Study

A study of the ramp rate on TAMU2 showed exceptional results. The quench current showed very little dependence on the ramp rate. The highest ramp rate requested was 2000 A/s and the quench current was 85% of the highest current found during the training quenches. Higher ramp rates were not requested due to power supply limitations.

Further examination of the data showed that the low inductance of the magnet, coupled with the feed back loop of the power supply, caused a very erratic performance of the power supply. The time average ramp rate was only 55% of requested; however, instantaneous graphs showed a different picture. The 8212 DAQ takes a data set 200 ms long which is centered on quench initiation. This unit detected instantaneous ramp rates as high as 4300 A/s for periods of 40ms without quenching. Two of the more dramatic graphs of current can be seen in figure 5.5.

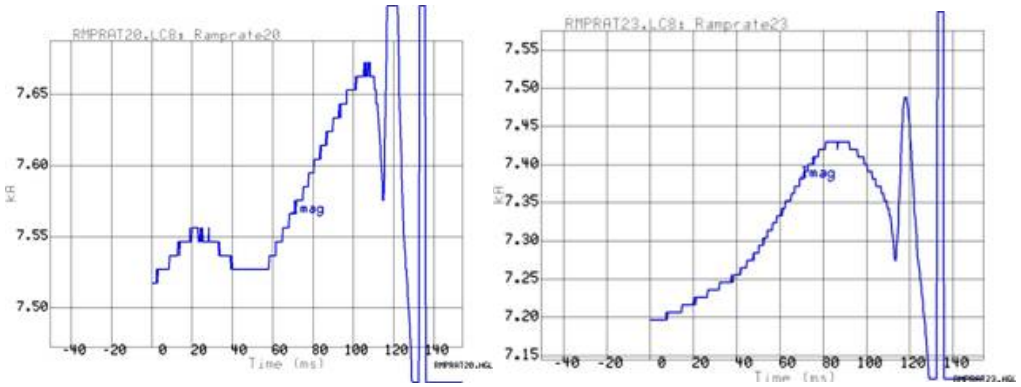

Fig. 5.5. Power supply fluxuations. Two graphs of the instantaneous performance of the power supply during the ramp rate tests.

5.5. Splices

Splice resistances were low and performed well. During testing the magnet was held at 8 kA while transducer measurements were taken. During this time it was noted that the temperature on the splices dropped while at this current level. Due to a voltage tap loss one of the leads could not be measured.

5.6. Coil End Loads

The loads on the coil ends were found to be a small fraction of the total calculated force. It is thought that much of the load was captured in tension inside the conductor itself. The coil ends are much like half of a solenoid magnet which holds some of its loads in tension as the conductor is already in a circular shape. Friction lock of the titanium beam should have aided the reduced load seen at the end transducer. Out of a potential 33.4 MPa possible, only 3.9 MPa was seen on the transducer.

This load was then held by the supporting steel block. The entire 3.9MPa was held in friction lock as design. The friction lock of the ends was confirmed by the bolt strain gauges which were designed to support any loads on the coil ends. The strain gauges measured no increase in loading throughout the entire test.

Table 5.1

Calculated possible stress levels and measured value for the ends of the magnet.

	Radial pressure on Transducer cross section
Calculated Inner Winding	13.2MPa
Calculated Outer Winding	20.2MPa
Vector sum Calculated	33.4MPa
Measured Pressure	3.9MPa

5.7. Lorentz Side Loads

The initial results of the side Lorentz load measurements were confusing. The two side transducers measured considerably different values. While the coil is asymmetric and this should be expected, the values should be close to each other. They were not. The five-blade transducer measured a total force close to 65MPa with a 10% error, which is well above the calculated maximum generated force of 46 MPa. The seven-blade transducer measured a more reasonable value. As a result of these measurements, further study of the coil and transducers was required to validate the results.

5.8. TAMU2 Cross-Section Study

After extraction from the flux return assembly, the TAMU2 coil was cut into multiple sections with a band saw. The sections were then carefully ground and lapped. Initially, the springs were of most interest as it appears they had failed and allowed the titanium beam to transmit loads directly to the outer winding. It was suspected that the springs had either filled with epoxy or had been crushed flat by the expanding titanium during reaction bake. Careful inspection revealed that both springs were intact and functional.

Several coil sections were then mounted onto the bed of a Bridgeport end mill. A microscope was then attached to the head of the mill so that careful measurements could be made with an accuracy of about .001". The locations of the various coil pieces were compared to the coil design and it was discovered that control over the winding package locations was not complete.

Both the inner and outer windings were over-compressed during the reaction bake cycle and as a result grew vertically. This extra horizontal room allowed for the springs on the right side of the magnet to expand by several thousandths and for the springs on the left side of the magnet to be only partially compressed.

Overall, the coil parts were close to their design locations and seemed to be functioning properly. The mica shear planes were broken and winding sections were easily removed. The only items that were not carefully examined in this process were the pressure transducers. The measurements from these sensors needed to be verified.

5.9. Transducer Tests

The final step in examining the performance of the TAMU2 magnet was a careful examination of the capacitive transducers used to measure the side Lorentz loads. A large hydraulic press was modified to operate at 25% of its capacity by removing most of the cylinders from the hydraulic circuit. Next a G-10 box and hammer were constructed for containing liquid nitrogen to cold test more pressure transducers. Three transducers were fabricated for testing.

The first transducer, #0 which was eventually fixed with epoxy onto a section of conductor taken from TAMU2, was cycled to pressures of up to 100 MPa at 300 K on the initial run but only 90 MPa on all subsequent runs. The materials in the transducers showed a tendency to cold flow which gives the device a memory which must be taken into consideration when analyzing the data taken from it. Tests at 72 K showed the materials in the sensor to cold flow as well but not nearly at severe at when at room temperature. At the low pressure region, the transducers become extremely sensitive and can change in excess of .1 nF.

The new data taken from the warm and cold tests allowed the Lorentz loading during the magnets tests to be determined with much greater accuracy. It is estimated that a pressure of 23.7 MPa was exerted on the seven-blade transducer during the magnet testing at Berkeley. The cold flowing of the transducer and the inaccuracy of the device measuring the seven blade transducer combine to give this measurement an error of 20%.

The five-blade transducer, which had measured a load greater than the total generated in the magnet, had been placed in negative compression which made it extremely sensitive. This gives the five-blade transducer an enormous error.

6. LESSONS

6.1. Fabrication Lessons

TAMU2 is the first Nb_3Sn dipole to be built at Texas A&M. To facilitate this, many procedures and techniques were developed for coil fabrication. A number of important changes were necessary for a successful test of the magnet. There were multiple issues which were solved during both while testing procedures and during coil fabrication.

6.1.1. Omega Temperature Controller

One of the simplest changes to the procedures pertains to a logic flaw found in the Omega temperature controllers used during the reaction bake of the magnet. The controllers operate in a full or zero power mode. To achieve 50% of total power the controller is on for 50% of the time cycle set by the user. During the ramp of the furnace the procedure that was developed requires low power from the controller as the furnace approaches the appropriate temperature. This procedure was necessary as the mass inside the furnace was very large when compared to the amount of heating power available. The magnet was inside the coffin throughout the reaction bake and experienced a considerable temperature change delay. As a result the controllers couldn't simply be set to the appropriate temperature. The magnet was slightly different from the dummy load used to test the procedure and so as the temperature approached 340°C, the controllers were set to zero power. It appears that as the controller attempts to turn on then off simultaneously, the off command is issued prior to the on command. This causes full power to be applied to the heaters instead of no power. Once the flaw was discovered, the furnace power was immediately cut and the gas flow to the coil was increased considerably. The coil temperature did overshoot but did not increase much beyond what was desired. To prevent this failure from reoccurring the lowest the controllers should be set is 1% power. At higher temperatures, 1% power is well below the amount of heat lost so the interior will cool.

6.1.2. Gasket Seals

A major benefit of the retort furnace that was constructed is that there are many parallel flow paths and controllable atmospheres possible. This is important as the bricks used for heat insulation can not be fully purged of oxygen and other undesirable gasses. Both the inner and outer windings had atmospheres independent of each other and the furnace. During a practice wind with dummy conductor cable, it was found that the outer winding could not be sealed fully and gas leaks were present. Although the parts were very smooth and machined precisely, small leaks were still present. Therefore a small amount of material on the steel that surrounded and was to seal the coil was removed by EDM. This allowed enough space for copper gaskets to be installed along the outer edges of the outer winding. With the application of these gaskets, the atmosphere inside the coils could be tightly controlled.

6.1.3. Coiled Copper Inflation lines

The bladder inflation process is delicate as the bladders themselves are fragile. The primary weak point of the bladders is the location where the stem blocks are welded to the stainless sheet that constitutes the inflatable bladder. A small hole is cut in the sheet and matched with the hole in the stem block. These two are then welded by laser to seal the junction. The stem extends out of the block and if force is applied, a considerable amount of torque is applied to the weld.

During the first attempt to load the magnet into the flux return structure, this weld point was stressed until it failed. As the bladder inflated, only the front section inflated due to the high viscosity of the Wood's metal. This angled the coil and the bladders which applied the stress on the weld joint. To prevent this from occurring, loops of small copper tubing were installed between the inflation fixture and the bladder stems. This allowed the bladders to move more freely while limiting the stress placed on the welded joints.

6.2. Changes to be Applied to TAMU3

6.2.1. Oven related pier damage

Because the Lorentz loads within TAMU2 were low, the damage to the pier and beam structure could be tolerated. The forces that will be in TAMU3 will require the Stress Management strategy to function properly. In an effort to prevent this damage from reoccurring, most of the titanium in the piers will be replaced with Inconel. Inconel will not distort like the titanium it is replacing as it has a superior heat transfer rate. The pier in the end regions of the coil will remain titanium for friction lock.

6.2.2. Coil Position within the Flux Return Laminations

As the TAMU program moves forward, field quality will become more of an issue. One of the issues that appeared with TAMU2 which must be solved is the location of the coil package within the flux return. The ideal position is in the center. The location will affect the field quality during ramp when the iron saturation front is moving through the flux return. The holes in the flux must be encountered symmetrically to prevent aberrations to the field.

To ensure the coil locations, hard mechanical stops will be installed on two of the four surfaces that interface with the bladders and coil in the flux return. The stops will limit the movement of the coils by preventing them from moving beyond a fixed measurement.

6.2.3. Potential Conductor Strain due to RTV in Mandrel Gap

While there is very little data suggesting that the conductor was strain damaged on the ends of the mandrel, that possibility exists in future magnets. The problem is from RTV jamming the gap in the mandrel partially open during reaction bake. If the conductor can not contract properly, stress can accumulate in the conductor near the ends of the mandrel, which is also the high field region.

To prevent this issue from becoming a problem, the laminations on either side of the gap will be slightly shorter than the rest of the mandrel. This will give room for a thin metal cap to prevent the gap from becoming a short to gas flow.

6.2.4. Transducer Calibration Issues

The data from the capacitive pressure transducers must be reliable for further verification of stress management in TAMU3. A press which is capable of calibrating the transducers at liquid nitrogen temperature, has now been completed. This will provide much closer readings to the data that comes from the transducers at 4 K. The transducers should also be kept under load at all times to minimize the cold flowing of the materials. Methods of cycling the transducers within the coil, after epoxy impregnation has taken place, should be looked into as well.

7. CONCLUSION

Overall, TAMU2, as a step along the path to a high field accelerator quality dipole, was very successful. A Nb_3Sn model dipole has been designed and fabricated at Texas A&M University. This dipole included unique features which provide the only presently known path of reaching far beyond 16 T record held today.

The primary goal of validating the Stress Management strategy has been realized in this low field test. It was initially thought that there had been a failure in the design of the magnet or implementation of Stress Management. With further investigation, it was discovered that an instrument error had made it only appear that the Lorentz loads from the inner winding were passing through the outer winding.

At these loads, the friction locking of axial forces has been successful as well. No change in loading from the bolt strain gages was measured throughout the testing at Berkeley. TAMU3 will provide a much more rigorous study of axial loads.

With this magnet, tooling was developed to facilitate quicker construction of future dipoles. Many of the fixtures had to be built and tested before there use. Many procedures have also been developed and modified throughout the fabrication process.

The testing of TAMU2 has shown that block coil dipoles are far less sensitive to ramp rates than are their cos θ or common coil counterparts. This could lead to a new series of rapid ramping dipoles which are needed for injectors and other experiments dealing with short lives particles.

REFERENCES

1. *Bevatron Magnet.* LBL News Magazine, 1981(Fall).
2. LHC Parameter and Layout Committee. *Parameters for MB*. Cryo Dipoles in the Arcs and the Dispersion 1999 [cited 2006 March 23]. Available from: http://edms.cern.ch/lhc_proj/plsql/lhcp.page?p_number=3054.
3. B. Benjegerdes, P. Bish, D. Byford, S. Caspi, D.R. Dietderich, et al., *Fabrication and test of Nb_3Sn racetrack coils at high field.* IEEE Transactions on Applied Superconductivity, 2001. 11(1): p. 2164-2167.
4. G.L. Sabbi, *Status of Nb_3Sn accelerator magnet R&D.* IEEE Transactions on Applied Superconductivity, 2002. 12(1): p. 236-241.
5. S. Mattafirri, S.C. Bartlett, P. Bish, S. Caspi, D.R. Dietderich, et al., *Performance analysis of HD1: a 16 Tesla Nb_3Sn dipole magnet.* IEEE Transactions on Applied Superconductivity, 2005. 15(2): p. 1156-1159.
6. C. Battle, R. Blackburn, N. Diaczenko, T. Elliott, R. Gaedke, et al. *Testing of TAMU1: A single-aperture block-coil dipole*. 2001.
7. A.F. Lietzke, S. Bartlett, P. Bish, S. Caspi, L. Chiesa, et al., *Test results for HD1, a 16 tesla Nb_3Sn dipole magnet.* IEEE Transactions on Applied Superconductivity, 2004. 14(2): p. 345-348.
8. A. Devred, S.A. Gourlay, and A. Yamamoto, *Future accelerator magnet needs.* IEEE Transactions on Applied Superconductivity, 2005. 15(2): p. 1192-1199.
9. A. Godeke, *Performance Boundaries in Nb_3Sn Superconductors*, in *Low Temperature Division Applied Superconductivity Center*. 2005, University of Twente University of Wisconsin-Madison. p. 215.
10. J. Ekin, *Mechanisms for critical-current degradation in NbTi and Nb_3Sn multifilamentary wires.* IEEE Transactions on Magnetics, 1977. 13(1): p. 127-130.
11. G. Moritz, *Fast-Pulsed Superconducting Magnets*, in *EPAC04*. 2004: Lucerne, Switzerland.
12. R.R. Hafalia, P. Bish, S. Caspi, D. Dietderich, S. Gourlay, et al., *A new support structure for high field magnets.* IEEE Transactions on Applied Superconductivity, 2002. **12**(1): p. 47-50.

13. A.D. McInturff, R.Benjegerdes, P. Bish, S. Caspi, K.Chow, et al. *Test results for a high field (13 T) Nb_3Sn dipole*. 1997.
14. A. den Ouden, S. Wessel, E. Krooshoop, H. ten Kate, et al., *Application of Nb_3Sn superconductors in high-field accelerator magnets.* IEEE Transactions on Applied Superconductivity, 1997. 7(2): p. 733-738.
15. A. McInturff, P. McIntyre, A. Sattarov. *Microbore Dipole for Future Hadron Colliders*. 2001. Snowmass CO.
16. R.W. Hanft, B. Brown, D. Herrup, M. Lamm, A. McInturff, et al., *Studies of time dependence of fields in Tevatron superconducting dipole magnets.* IEEE Transactions on Magnetics, 1989. 25(2): p. 1647-1651.
17. B. Seeber, *Handbook of applied superconductivity*. 1998, Bristol ; Philadelphia: Institute of Physics Pub. 2 v. (xxiv, 1912, [47] p.).
18. B. Brown, H. Fisk, and R. Hanft, *Persistent current fields in Fermilab Tevatron magnets.* IEEE Transactions on Magnetics, 1985. 21(2): p. 979-982.
19. D. Herrup, M. Syphers, D. Johnson, R. Johnson, A. Tollestrup, et al., *Time variations of fields in superconducting magnets and their effects on accelerators.* IEEE Transactions on Magnetics, 1989. 25(2): p. 1643-1646.
20. L. Bottura, L. Walckiers, and R. Wolf, *Field errors decay and “snap-back” in LHC model dipoles.* IEEE Transactions on Applied Superconductivity, 1997. **7**(2): p. 602-605.
21. N. Diaczenko, T. Elliott, W. Henchel, E. Hill, M. Johnson, et al., *Construction of a 13 Tesla hybrid block-coil dipole for future hadron colliders.* IEEE Transactions on Applied Superconductivity, 2001. 11(1): p. 2264-2267.
22. A. Abreu, C.Battle., G. Cryer, N. Diaczenko, T. Elliott, H. Eucker, et al., *Block Dipole for Future Hadron Colliders*. IEEE Transactions on Applied Superconductivity. 1998. Palm Desert, CA.

VITA

Name:	Patrick Daniel Noyes
Address:	National High Magneic Field Laboratory, 1800 E. Paul Dirac Dr. Tallahassee, FL 32310
Email Address:	noyes@magnet.fsu.edu
Education:	B.S. in Physics, Texas A&M University, 2001 M.S. in Physics, Texas A&M University, 2007